2020 Offshore Wind Resource Assessment for the California Pacific Outer Continental Shelf

Mike Optis, Alex Rybchuk, Nicola Bodini, Michael Rossol, and Walter Musial

National Renewable Energy Laboratory

Produced under direction of the Bureau of Ocean Energy Management (BOEM) by the National Renewable Energy Laboratory (NREL) under Interagency Agreement IAG-19-2123.

NREL is a national laboratory of the U.S. Department of Energy
Office of Energy Efficiency & Renewable Energy
Operated by the Alliance for Sustainable Energy, LLC

This report is available at no cost from the National Renewable Energy Laboratory (NREL) at www.nrel.gov/publications.

Contract No. DE-AC36-08GO28308

Strategic Partnership Project Report
NREL/TP-5000-77642
OCS Study BOEM 2020-043
October 2020

2020 Offshore Wind Resource Assessment for the California Pacific Outer Continental Shelf

Mike Optis, Alex Rybchuk, Nicola Bodini, Michael Rossol, and Walter Musial

National Renewable Energy Laboratory

Suggested Citation
Optis, Mike, Alex Rybchuk, Nicola Bodini, Michael Rossol, and Walter Musial. 2020. *2020 Offshore Wind Resource Assessment for the California Pacific Outer Continental Shelf*. Golden, CO: National Renewable Energy Laboratory. NREL/TP-5000-77642. https://www.nrel.gov/docs/fy21osti/77642.pdf.

NREL is a national laboratory of the U.S. Department of Energy
Office of Energy Efficiency & Renewable Energy
Operated by the Alliance for Sustainable Energy, LLC

This report is available at no cost from the National Renewable Energy Laboratory (NREL) at www.nrel.gov/publications.

Contract No. DE-AC36-08GO28308

Strategic Partnership Project Report
NREL/TP-5000-77642
OCS Study BOEM 2020-043
October 2020

National Renewable Energy Laboratory
15013 Denver West Parkway
Golden, CO 80401
303-275-3000 • www.nrel.gov

NOTICE

This work was authored by the National Renewable Energy Laboratory, operated by Alliance for Sustainable Energy, LLC, for the U.S. Department of Energy (DOE) under Contract No. DE-AC36-08GO28308. Support for the work was also provided by the U.S. Department of Interior (DOI), Bureau of Ocean Energy Management (BOEM) under Agreement No. IAG-19-2123. The views expressed in the article do not necessarily represent the views of the DOE or the U.S. Government. The U.S. Government retains and the publisher, by accepting the article for publication, acknowledges that the U.S. Government retains a nonexclusive, paid-up, irrevocable, worldwide license to publish or reproduce the published form of this work, or allow others to do so, for U.S. Government purposes.

Cover Photos by Dennis Schroeder: (clockwise, left to right) NREL 51934, NREL 45897, NREL 42160, NREL 45891, NREL 48097, NREL 46526.

Acknowledgments

This work was supported and funded by the Bureau of Ocean Energy Management (BOEM). We would like to thank the BOEM Pacific leadership team, including Sara Guiltinan, Necy Sumait, Joan Barminski, Douglas Boren, and Jean Thurston-Keller for supporting this research and providing feedback throughout the process. We would also like to thank Angel McCoy for BOEM's federal support of this work. The National Renewable Energy Laboratory (NREL) acknowledges the New York State Energy Research and Development Authority for the public dissemination of floating lidar data, which were critical for this analysis. We would like to thank Weiming Hu from the Geoinformatics and Earth Observation Laboratory at Penn State University for assisting with the analog ensemble analysis and for the use of the PAnEn codebase for running analog ensembles. Finally, NREL would also like to thank the following peer reviewers for increasing the quality of this report: Will Shaw (Pacific Northwest National Laboratory), Arne Jacobson and Mark Severy (Humboldt State University), David Miller (California Public Utilities Commission), Adam Stern (Offshore Wind California), Yi-Hui Wang (California Polytechnic State University), Cindy Whitten (Federal Aviation Administration), Eli Harland and Scott Flint (California Energy Commission), and Chris Potter (California Ocean Protection Council). Technical editing and support were provided by Sheri Anstedt and Tiffany Byrne.

Acronym List

AGL	above ground level
AnEn	analog ensemble
BOEM	Bureau of Ocean Energy Management
DOE	U.S. Department of Energy
ECMWF	European Centre for Medium-Range Weather Forecasts
EMD	earth mover's distance
ERA5	ECMWF Reanalysis Version 5
IAV	interannual variability
LSM	land surface model
MERRA-2	Modern-Era Retrospective analysis for Research and Applications, Version 2
MYNN	Mellor-Yamada-Nakanishi-Niino
NASA	National Aeronautics and Space Administration
NCEP	National Center for Environmental Prediction
NDBC	National Data Buoy Center
NEWA	New European Wind Atlas
NOAA	National Oceanic and Atmospheric Administration
Noah-MP	Noah-Multiparameterization
NREL	National Renewable Energy Laboratory
NWP	numerical weather prediction
NYSERDA	New York State Energy Research and Development Authority
OCS	Outer Continental Shelf
OSTIA	Operational Sea Surface Temperature and Sea Ice Analysis
PBL	planetary boundary layer
R&D	research and development
RMSE	root-mean-square error
RTG	Real-Time Global
SST	sea-surface temperature
USGS	U.S. Geological Survey
WIND	Wind Integration National Dataset
WRF	Weather Research and Forecasting (model)
WTK	Wind Integration National Dataset Toolkit
YSU	Yonsei University

Executive Summary

This report presents a state-of-the-art wind resource data set produced by the National Renewable Energy Laboratory (NREL) for the outer continental shelf (OCS) off the coast of California.[1] This data set — referred throughout this report as CA20 — replaces NREL's Wind Integration National Dataset (WIND) Toolkit for the OCS, which was produced and released publicly in 2013 and is currently the principal data set used by stakeholders for wind resource assessment in the continental United States. Both the WIND Toolkit and the CA20 data set are created using the Weather Research and Forecasting (WRF) numerical weather prediction (NWP) model.

This update to the OCS wind resource data set is part of a larger study funded by the Bureau of Ocean Energy Management (BOEM) that will provide an updated cost model for floating offshore wind in the OCS. Currently in a precommercial phase, commercial floating offshore wind technology will be available for the California market by the mid-2020s.

In order to provide accurate cost estimates for floating wind in the California OCS, a new wind resource data set was required. Since the release of the WIND Toolkit in 2013, extensive research and development (R&D) in NWP models and especially the WRF model has been performed. This R&D includes:

- Dedicated large-scale field campaigns aimed specifically at improving WRF for wind energy applications in simple and complex terrain (Wilczak et al. 2015; Shaw et al. 2019)
- The release of state-of-the-art global atmospheric products used as boundary forcings in WRF (León 2019)
- Growing research demonstrating the sensitivity in NWP-modeled wind speeds to different model inputs and parameterizations (Hahmann et al. 2020)
- Increased understanding that long-term wind resource data sets of at least 20 years are required for robust long-term analyses, such as estimating annual energy production and interannual variability (IAV).

NREL has developed and disseminated an updated wind resource data set for the OCS that leverages these R&D advancements. The CA20 data set shares many of the same attributes as the WIND Toolkit, including 5-minute time resolution and 2-kilometer (km) horizontal spatial resolution. However, the CA20 data set improves upon the WIND Toolkit through:

1. A 20-year modeling period from 2000 through 2019 (compared to the 7-year 2007–2013 modeling period in the WIND Toolkit)
2. A sensitivity analysis of the hub-height wind resource, driven by an ensemble of 16 different WRF simulations run in the 2017 calendar year
3. An updated WRF model, from Version 3.4 used in the WIND Toolkit to Version 4.1.2 used here, which incorporates significant R&D advancements
4. The use of the state-of-the-art reanalysis product ERA5 to provide atmospheric forcing at the WRF domain boundaries. The ERA5 product is produced by the European Centre for Medium-Range Weather Forecasts (ECMWF) and replaces its older ERA-Interim product, which was used in the WIND Toolkit.

The updated annual average wind resource map for the OCS is shown in Figure A. Similar to the WIND Toolkit, the north of the domain has the highest wind resource while the south has a more moderate resource. As shown in the figure, the lowest part of the U.S. Exclusive Economic Zone that extends into Mexico is not considered relevant and is therefore not included in this report.

The mean annual 100-m wind speeds from the CA20 data set are compared with those from the WIND Toolkit in Figure B. The CA20 data set indicates significantly higher mean wind speeds than the WIND Toolkit. In some areas, the increase is nearly 2 meters per second ($m \cdot s^{-1}$), or an increase of about 20%. As indicated in Table A, increases

[1] For the purposes of this report, the OCS refers to the offshore area from 0 to 200 nautical miles off the California coast.

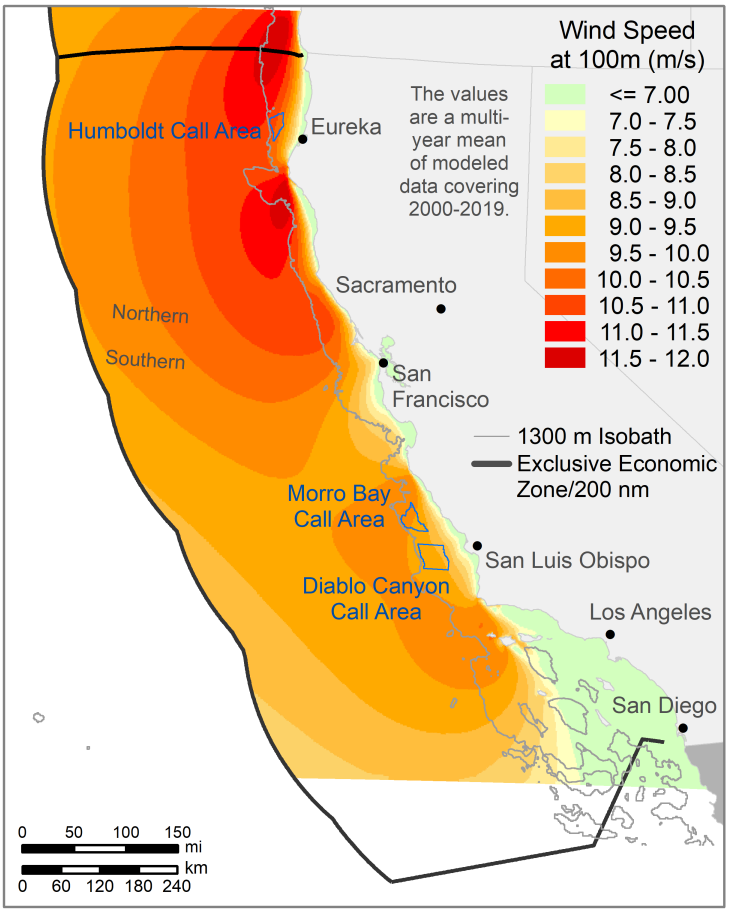

Figure A. Mean annual wind resource for the OCS based on the new 20-year data set

in the mean 100-meter (m) wind speed at the centroids of current wind energy Call Areas[2] are 10.6%, 16.1%, and 19.2% at Humboldt, Morro Bay, and Diablo Canyon, respectively.

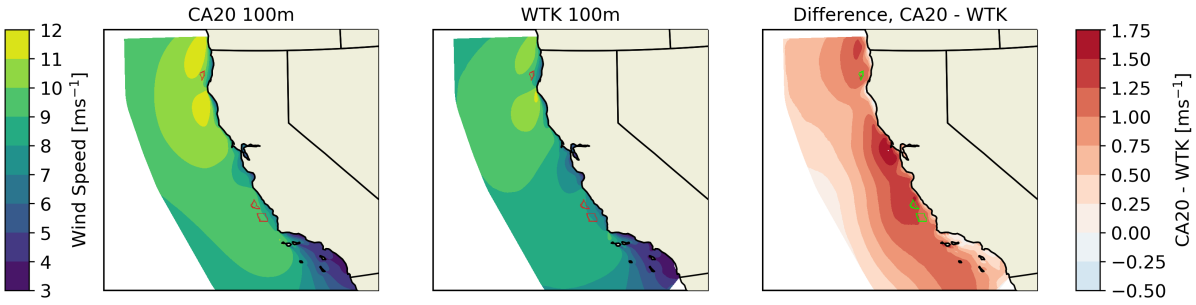

Figure B. Comparing the mean annual 100-m wind speeds from the CA20 data set, labeled CA20 (left), and the WIND Toolkit, labeled WTK (center). The difference between the two maps is calculated in the rightmost figure.

This increase in the modeled wind resource is significant and will impact economic and energy modeling and planning for offshore wind in the OCS. Therefore, this report is largely focused on explaining and justifying this increase in the modeled resource, primarily through validation against observations and examining the underlying differences between the new CA20 data set and the WIND Toolkit model setups.

Table A. Comparison of Mean Annual 100-m Wind Speeds between the WIND Toolkit and the New 20-Year Data Set at the Offshore California Call Area Centroids

Call Area	Mean Wind Speed (m·s^{-1})		Change	
	WIND Toolkit	Updated Data Set	(m·s^{-1})	(%)
Humboldt	9.41	10.41	1.00	10.6
Morro Bay	8.20	9.52	1.32	16.1
Diablo Canyon	7.70	9.18	1.48	19.2

Based on this detailed analysis, much of the increase in the wind resource can be attributed to an updated planetary boundary layer (PBL) scheme. The PBL scheme is a critical parameterization in the WRF model. It controls how turbulence distributes momentum in the lower part of the atmosphere and strongly influences the wind shear profiles. The WRF model currently has nine possible PBL schemes. The WIND Toolkit used the Yonsei University (YSU) scheme, whereas the CA20 data set uses the Mellor-Yamada-Nakanishi-Niino (MYNN) scheme. The MYNN scheme has been the subject of significant research and development over the past decade and has become the global standard for wind resource assessment. The use of the MYNN scheme produces significantly higher hub-height wind speeds than YSU, which can be attributed to the high frequency of stable atmospheric conditions in the OCS and the divergence of these PBL schemes under such conditions.

However, the change in PBL scheme is not sufficient to fully account for the change in the wind resource. Even after considering the impact of an updated reanalysis product, longer time period, updated WRF version, and updated sea-surface temperature product, there remains an unaccounted 0.98- and 1.11-m·s^{-1} increase at the Morro Bay and Diablo Canyon Call Areas, respectively; by contrast, only 0.17 m·s^{-1} is left unaccounted at Humboldt. The unaccounted values are likely caused by other differences between CA20 and WTK not explored in this analysis, including different topographic and land use data and different domain sizes (WTK used a domain covering the entire continental United States).

[2]Call Areas refer to areas identified by BOEM in 2018 as potentially suitable for offshore wind energy leasing and were under consideration for offshore wind energy as of the publication of this report.

The resource assessment using the CA20 wind resource data indicates an increase in technical potential for the OCS, summarized in Table B.[3] This increase in technical potential is based on comparisons with NREL's 2016 U.S. wind energy resource assessment (Musial et al. 2016). Overall, we find an increase of 34% in technical potential, most of which is attributable to additional exclusions included in the 2016 analysis but not applied here (see Section 3.2 for more details). Some of the increase is also attributed to an increased depth limit from 1,000 m to 1,300 m for floating wind installations, which reflects potential advancements in floating wind mooring technologies (Figure C). Finally, about 4.7% of the increase in technical potential is attributed to the increase in the modeled wind resource.

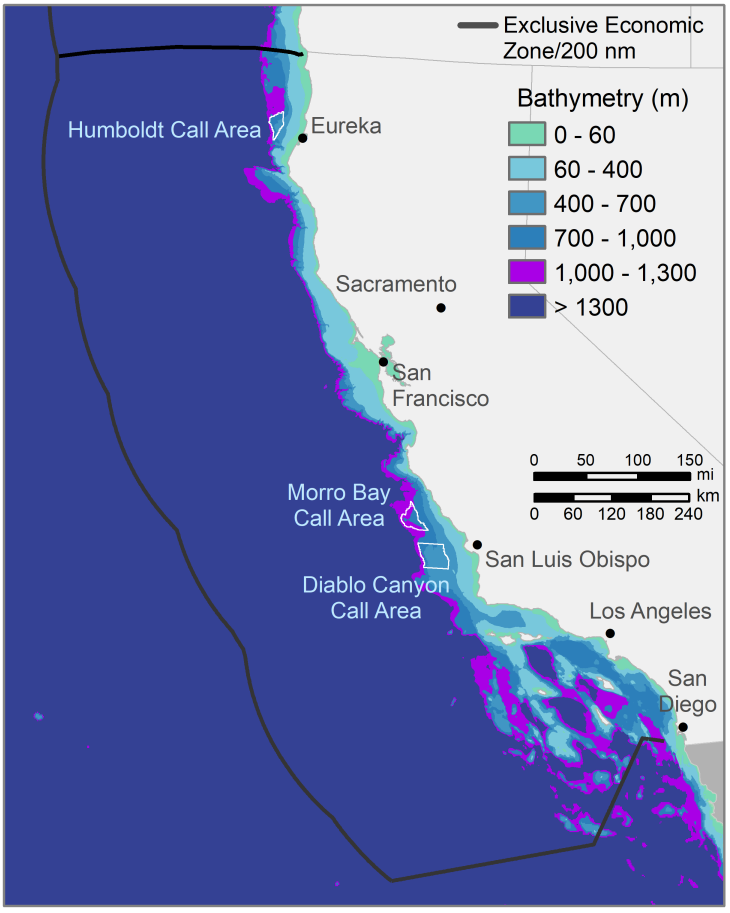

Figure C. Bathymetry of the OCS up to 1,300 m, based on data from the National Oceanic and Atmospheric Administration's Coastal Relief Model

The significant increase in the modeled wind resource compared to the WIND Toolkit highlights the sensitivity of NWP-modeled wind speeds to model inputs and setup (e.g., reanalysis product and PBL scheme). Since 2018, NREL has been developing methods to quantify this sensitivity and disseminate this information with its wind resource products in order for stakeholders to better use and understand the uncertainty around modeled wind resource data sets. The wind resource data set here is a culmination of those efforts. To quantify the sensitivity of this modeled OCS wind resource data set, NREL considered an ensemble of WRF setups that vary in the inputs and model parameterizations within WRF. Specifically, 16 different setups to the WRF model are used to run simulations over

[3] A detailed description of technical potential can be found in Musial et al. 2016, but briefly, technical potential is the amount of offshore wind capacity that could be developed while taking into account exclusion factors related to water depth, mean wind speed, industry uses, and environmental conflicts. By contrast, gross potential is the capacity without these exclusions.

Table B. Comparison of Gross and Technical Potential Estimates from 2016 Report and This Report

Metric	2016 Report	This Report	
		WIND Toolkit	New CA20 Data Set
Minimum average wind speed ($m \cdot s^{-1}$)	7.0	7.0	7.0
Maximum water depth (m)	1,000	1,300	1,300
Array density ($MW \cdot km^{-2}$)	3.0	3.0	3.0
Gross potential (km^2)	566,058	566,058	566,058
Gross potential (gigawatts [GW])	1,698	1,698	1,698
Technical potential (km^2)	49,916	64,048	67,067
Technical potential (GW)	150	192	201

the 2017 calendar year, which was found to have the strongest coverage of observational data in the OCS and therefore best suited for validation. These setups account for such commonly used reanalysis products as boundary forcing, different PBL schemes, different sea-surface temperature forcing products, and different land surface schemes. The spread of modeled 100-m wind speeds is quantified from these different model setups—both on annual and hourly scales—as the standard deviation of modeled winds divided by their mean (i.e., the coefficient of variation). This metric calculated for the calendar year 2017 is extended to the 20-year data set by training a machine-learning model to predict this sensitivity from key modeled atmospheric variables. This novel approach developed by NREL is then contrasted against a traditional analog ensemble approach in which sensitivity is deduced from a single model run without the use of actual ensembles.

The sensitivity in the annual wind resource based on the coefficient of determination is shown in Figure D. Annual sensitivities range between 1% and 7% and are highest near the coastline and around the wind energy Call Areas. Most of the sensitivity shown is attributable to the choice of PBL scheme used to run the WRF model. These values can be interpreted as NREL's confidence in the modeled wind resource at each grid point.

The creation of a 20-year data set, as well as 16 ensemble setups run over a year, are made possible by investment in both computational resources and atmospheric science expertise at NREL. The methods and framework developed to produce this CA20 data set are currently being leveraged to begin the full replacement of the national-scale WIND Toolkit, which is expected to be complete in 2022.

There is currently a rapid pace of R&D in NWP science, with an emphasis on improving offshore wind resource modeling. This research is critical given the current and likely continuing scarcity of U.S. offshore hub-height wind observations, and therefore the increased reliance on modeled data. As the United States and the world become more and more dependent on weather-driven renewable resources, an ever-greater understanding of the offshore wind resource and how it interacts with emerging offshore wind technology is required. Given this need, NREL is developing the capacity and framework to continually update its wind resource modeling capabilities and products, likely on 5- to 7-year update periods. These frequent updates will ensure that the most accurate and comprehensive wind resource data sets for U.S. and global markets are available to wind energy stakeholders.

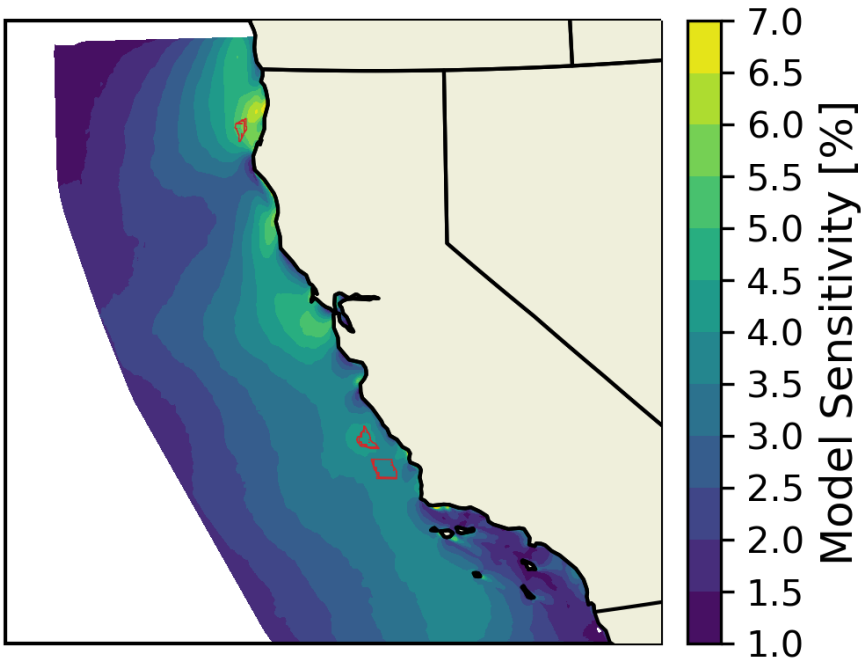

Figure D. Sensitivity in the modeled 100-m wind resource, quantified as the coefficient of variation—or standard deviation divided by the mean—across the different mean wind speeds modeled from the 16 different ensembles. Wind energy Call Areas are shown in red.

Table of Contents

List of Figures

List of Tables

1 Introduction

This report presents a state-of-the-art wind resource data set produced by the National Renewable Energy Laboratory (NREL) for the outer continental shelf (OCS) off the coast of California.[1] This update to the OCS wind resource data set is part of a larger study funded by the Bureau of Ocean Energy Management (BOEM) to provide an updated cost model for floating offshore wind in the OCS. Currently in a precommercial phase, commercial floating offshore wind technology will be available for the California market by the mid-2020s.

This new wind resource data set (referred to as CA20 throughout this report) replaces NREL's Wind Integration National Dataset (WIND) Toolkit for use in the OCS. The WIND Toolkit was produced in 2013 using the Weather Research and Forecasting (WRF) numerical weather prediction (NWP) model. The WIND Toolkit is a 7-year data set (2007–2013) run at 2-kilometer (km) horizontal spatial resolution and 5-minute time resolution that covers the entire continental United States. Modeled variables include wind speed, wind direction, and temperature at multiple heights up to 200 m, as well as relevant surface meteorological variables. Data are publicly disseminated at no cost through NREL's Wind Prospector tool and is hosted on Amazon Web Services.

Since 2013, the WIND Toolkit has served as the most comprehensive publicly available wind resource data set in the United States (Draxl et al. 2015; Draxl and Hodge 2015). It has been used by various stakeholders ranging from wind energy developers and consultants, utilities, government organizations, and academic and research institutions. Given this extensive use of the WIND Toolkit, NREL is committed to ensuring that its NWP modeling capabilities remain state of the art and that NREL continues to provide the most accurate wind resource information possible to its partners and stakeholders.

With this in mind, NREL is currently in the process of replacing the WIND Toolkit with a next-generation, state-of-the-art NWP data set. Since the release of the WIND Toolkit in 2013, extensive research and development (R&D) in NWP models, and especially the WRF model, has been performed within the global atmospheric modeling community. Such development includes:

- Dedicated large-scale field campaigns aimed specifically at improving WRF for wind energy applications in simple and complex terrain (Wilczak et al. 2015; Shaw et al. 2019)
- The release of state-of-the-art global atmospheric products used as boundary forcings in WRF (León 2019)
- Growing research demonstrating the sensitivity in NWP-modeled wind speeds to different model inputs and parameterizations (Hahmann et al. 2020)
- Increased understanding that long-term wind resource data sets of at least 20 years are required for robust long-term analyses, such as estimating annual energy production.

NREL has developed and disseminated an updated wind resource data set for the OCS that leverages these R&D advancements. This report describes the creation of this new CA20 data set, focusing mainly on:

1. The use of a 20-year modeling period from 2000–2019
2. Detailed validation of model results against buoys, coastal radars, and offshore floating lidars
3. The use of 16 different WRF model setups or ensembles to (a) determine the best-performing model setup for use in the 20-year production run and (b) quantify the sensitivity in the modeled resource by running all ensembles over a single calendar year
4. A detailed comparison between modeled winds in the CA20 data set and the WIND Toolkit, with any differences clearly justified and explained
5. Presenting novel machine-learning techniques to extrapolate model sensitivity quantified in a single calendar year to the full 20-year time period.

[1] The OCS refers to the offshore area from 0 to 200 nautical miles off the California coast.

The creation of a 20-year data set as well as 16 ensemble setups run over a year require extensive high-performance computational resources as well as an in-depth understanding of boundary layer atmospheric science. The methods and framework developed to produce the CA20 data set are currently being leveraged to begin the full replacement of the national-scale WIND Toolkit, which is expected to be complete some time in 2022.

There is currently a rapid pace of R&D in NWP science, with an emphasis on improving offshore wind resource modeling. This research is critical given the current and likely continuing scarcity of U.S. offshore hub-height wind observations, and therefore the increased reliance on modeled data. As the United States and the world become more and more dependent on weather-driven renewable resources, an ever-greater understanding of the offshore wind resource and how it interacts with emerging offshore wind technology is required. Given this need, NREL is developing the capacity and framework to continually update its wind resource modeling capabilities and products, likely on 5- to 7-year update periods. These frequent updates will ensure that the most accurate and comprehensive wind resource data sets for U.S. and global markets are available to wind energy stakeholders.

2 Motivation for CA20 Data Set

In this section, we describe the development of the new CA20 wind resource data set. First, we describe the 16 different WRF model setups, or ensemble members, that are considered for use in the full 20-year data set. Each setup is used to simulate the OCS wind resource in the 2017 calendar year, which was found to have the best coverage of observational data for model validation. Simulation results are compared against buoy and coastal radar observations in California. Because of the lack of floating lidar in the OCS, simulations are also compared against two floating lidars in the New Jersey wind energy offshore area in the Atlantic Ocean. Based on the validation results, the selection of the final model setup for the 20-year production run is presented and discussed in detail.

2.1 Constructing the Different Model Setups

The WRF model is highly modular in that it allows users to consider a range of inputs (e.g., atmospheric forcing, sea-surface temperature [SST] forcing), parameterizations (e.g., radiation schemes, land surface schemes), grid specifications (e.g., vertical and horizontal resolution), and a large range of physics and dynamics settings (e.g., time steps) (Skamarock et al. 2019). This model flexibility allows users to design a model setup that best suits the desired application. However, this flexibility allows for a virtually unlimited set of reasonable model setups, all of which, to some extent, will produce different outputs.

In this context, it is crucial to understand which components strongly impact modeled hub-height winds so that accurate and reliable wind resource data are produced. Over a decade of research into this topic has demonstrated sensitivity in NWP-modeled wind speeds to the planetary boundary layer (PBL) scheme (Ruiz, Saulo, and Nogués-Paegle 2010; Carvalho et al. 2014b; Gómez-Navarro, Raible, and Dierer 2015; Hahmann et al. 2015; Olsen et al. 2017; Siuta, West, and Stull 2017), the large-scale atmospheric forcing ("WRF wind simulation and wind energy production estimates forced by different reanalyses: Comparison with observed data for Portugal" 2014; Carvalho et al. 2014a; Hahmann et al. 2015; Siuta, West, and Stull 2017), data assimilation techniques (Ulazia, Saenz, and Ibarra-Berastegui 2016), nesting techniques (Gómez-Navarro, Raible, and Dierer 2015), grid size (Siuta, West, and Stull 2017), vertical resolution (Hahmann et al. 2015), horizontal resolution (Olsen et al. 2017), spin-up time (Hahmann et al. 2015), SST (Hahmann et al. 2015), convection schemes (Ruiz, Saulo, and Nogués-Paegle 2010), and soil models (Ruiz, Saulo, and Nogués-Paegle 2010). The most exhaustive sensitivity analysis to date was recently published as part of the development of the New European Wind Atlas (NEWA) (Hahmann et al. 2020). Similar in scope to the WIND Toolkit, the NEWA is a 30-year WRF-based data set covering all of Europe. NREL recently completed an offshore study of WRF model sensitivity in partnership with Rutgers Center for Ocean Observing Leadership (Optis et al. 2020). Results from this study support previous research findings and found that the PBL scheme, reanalysis forcing, and SST forcings were all key drivers of model sensitivity, especially on short timescales.

Based on this literature review and NREL's previous experience on WRF sensitivity in offshore wind resource modeling, a total of 16 model setups are constructed based on variations in four key model components. These components are summarized in Table 1 and described here:

1. **Reanalysis forcing product**: WRF-modeled wind speeds can be very sensitive to the large-scale global atmospheric product used as boundary forcing to the model. In this study, we consider the use of the ERA5 reanalysis product developed by the European Centre for Medium-Range Weather Forecasts (ECMWF) (Hersbach et al. 2020) and the Modern-Era Retrospective analysis for Research and Applications, Version 2 (MERRA-2) (Gelaro et al. 2017), developed by the National Aeronautics and Space Administration (NASA). These two data sets represent state-of-the-art reanalysis products and are widely used in the wind industry for wind resource characterization. ERA5 is run at $0.25^o \times 0.25^o$ horizontal resolution with 137 vertical levels and data output every hour. MERRA-2 is run at $0.50^o \times 0.625^o$ horizontal resolution with 72 vertical levels and data output every hour.
2. **PBL scheme**: The PBL scheme is a critical parameterization in the WRF model. It controls how turbulence distributes momentum in the lower part of the atmosphere and strongly influences the shape of wind profiles. The WRF model currently has nine possible PBL schemes to select. In this study, we consider both the Mellor-

Yamada-Nakanishi-Niino (MYNN) and Yonsei University (YSU) PBL schemes, which are widely considered the two most popular PBL schemes in WRF. The YSU scheme was used in the WIND Toolkit, while the MYNN scheme is widely used in modern wind resource products (Hahmann et al. 2020) and operational forecast products (Benjamin et al. 2016) and has been the focus of R&D efforts and improvements through U.S. Department of Energy (DOE)-funded large-scale field campaigns: the Wind Forecast Improvement Projects (Wilczak et al. 2015; Shaw et al. 2019).

3. **SST product**: The WRF model does not compute SST or any water surface temperatures; rather, these data are provided as input to WRF and act as a lower boundary forcing. Both the ERA5 and MERRA-2 reanalysis products include SST data produced from the Operational Sea Surface Temperature and Sea Ice Analysis (OSTIA) data set produced by the UK Met Office (Donlon et al. 2012; Hirahara et al. 2016; Bosilovich 2015). The OSTIA data are provided at $1/20^o$ horizontal spatial resolution. In addition to the OSTIA data set, we consider the use of the National Center for Environmental Prediction (NCEP) Real-Time Global (RTG) SST product (Grumbine 2020). This product has a spatial resolution of $1/12^o$.
4. **Land surface model (LSM)**: Unlike water surfaces, land surface temperatures are modeled in WRF using land surface models. These models simulate the exchange of energy and water fluxes between the surface and atmosphere and can have significant influence on offshore coastal winds given the role of the land temperature in the sea breeze. We consider two LSM schemes: the Noah LSM and the updated Noah-Multiparameterization (Noah-MP) LSM (Niu et al. 2011).

Table 1. WRF Model Components Used To Construct the 16-Member Ensemble in This Validation Study

Category	Values Considered for WRF Ensemble
Atmospheric forcing	MERRA-2 ERA5
Planetary boundary layer scheme	MYNN YSU
Sea-surface temperature forcing	OSTIA NCEP RTG
Land surface model	Noah Noah-MP

2.2 Running the Simulations

Each of the WRF model setups described in Section 2.1 share other common attributes, which are summarized in Table 2. These attributes include high vertical resolution with nine levels below 200 m, allowing for accurate resolution of wind profiles. To downscale the large-scale forcing to 2 km, we use a nested WRF domain comprising a large 6-km domain in which the higher-resolution 2-km domain is placed. The boundary forcing provided by the reanalysis product is applied only to the 6-km domain, whose output becomes the boundary forcing to the 2-km domain. The 2-km domain covers the OCS out to the 200-nautical-mile U.S. Exclusive Economic Zone, as shown in Figure 1.

We ran each of the 16 model setups over the 2017 calendar year. We select this year because of strong data coverage from the observational network (described in Section 2.2.1). To leverage parallel computing and shorten the overall simulation time, we perform WRF simulations separately for each month and then concatenate the data into a single time series at each grid location during postprocessing. A spin-up period of 2 days is used prior to the simulations (e.g., February simulations started on January 30) to allow the model to develop sufficiently from the initial conditions and stabilize.

For long simulation periods, such as a month, it is common for an inner WRF domain to "drift away" from the large-scale atmospheric forcing applied only at the outer domain boundary. To correct for this, it is common to apply atmospheric nudging in the model—a form of data assimilation that occasionally adjusts dynamical variables in WRF toward the large-scale flow. Atmospheric nudging is applied in this analysis to the 6-km domain only using spectral-based nudging applied every 6 hours.

For all simulations, we use WRF Version 4.1.2, released in July 2019. A detailed WRF "namelist" that provides the full specifications of the WRF model used here will be published online through zenodo.org[1] upon final publication of this report.

Table 2. Common Attributes in the WRF Ensembles Considered in this Analysis

Feature	Specification
WRF version	4.1.2
Nesting	6 km, 2 km
Vertical levels	61
Near-surface-level heights (meters)	12, 34, 52, 69, 86, 107, 134, 165, 200
Atmospheric nudging	Spectral nudging on 6-km domain, applied every 6 hours
Microphysics	Ferrier
Longwave radiation	Rapid Radiative Transfer Model
Shortwave radiation	Rapid Radiative Transfer Model
Topographic database	Global Multi-Resolution Terrain Elevation Data from the United States Geological Service and National Geospatial-Intelligence Agency
Land-use data	Moderate Resolution Imaging Spectroradiometer 30s
Cumulus parameterization	Kain-Fritsch

2.2.1 Observations

A network of observations is used to validate the different WRF model setups in the OCS. These observations—summarized in Table 3 and shown on the domain map in Figure 1—include:

1. Buoy-based measurements of wind speed provided by the National Data Buoy Center (NDBC), operated by the National Oceanic and Atmospheric Administration (NOAA).[2] Buoy measurements are either at 3.8 or 4.1 meters above water level.
2. Coastal radar measurements from the NOAA profiler network.[3] Several sites along the California coast are used, which provide hourly average wind speed measurements starting at heights in the 150–200-m range and extending several kilometers up into the atmosphere.

These observation stations are not ideal for validating modeled offshore wind speeds at hub height. Buoys only measure wind speeds a few meters above water level; given the different wind regimes at the surface and aloft, it is uncertain if relative model performance at 5 m or below would hold at hub height. By contrast, the radars measure at more relevant heights for wind energy. However, they are located at the interface between the ocean and land. As such, they are subject to large wind-speed gradients that hinder NWP validation efforts. Under these conditions, modeled wind speeds from one model grid box to the next can change significantly, and the interpolation of modeled

[1]Zenodo is an open-access repository that allows researchers to store data sets, software, reports, and other relevant digital information.
[2]https://www.ndbc.noaa.gov/
[3]https://psl.noaa.gov/data/obs/datadisplay/

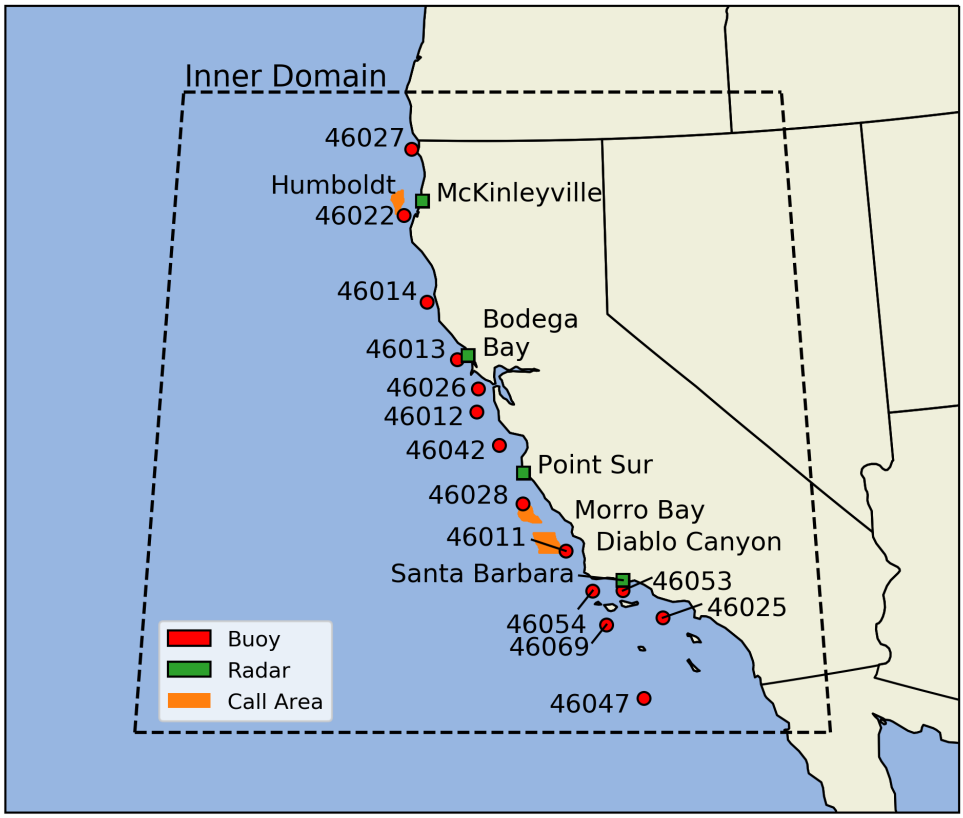

Figure 1. The spatial domain of the 2-km WRF simulations for the OCS (dotted line), the buoy (red) and radar (green) observation stations used for validation, and the current wind energy Call Areas (orange)

Table 3. List of Buoy and Coastal Radar Stations Used for Validating WRF Simulations in the OCS

Name	Type	Height (m)
46025	Buoy	4.1
46027	Buoy	3.8
46026	Buoy	3.8
46022	Buoy	3.8
46047	Buoy	3.8
46053	Buoy	4.1
46069	Buoy	4.1
46054	Buoy	3.8
46042	Buoy	4.1
46011	Buoy	4.1
46012	Buoy	3.8
46013	Buoy	4.1
46014	Buoy	3.8
46028	Buoy	4.1
Bodega Bay	Radar	195
Santa Barbara	Radar	193
Point Sur	Radar	195
McKinleyville	Radar	195

wind speeds to the observation station for purposes of validation becomes uncertain. A more detailed discussion and analysis of this coastal gradient issue at the radar locations is provided in the Appendix.

Floating lidar measurements from buoys in the OCS would provide the ideal validation measurements because of their relevant locations (i.e., close or within wind energy Call Areas) and relevant hub-height measurements. However, no such measurements in the OCS were available to NREL for this study. By contrast, there are several private and public deployments of floating lidar within and adjacent to offshore wind Lease Areas and Call Areas in the Atlantic. Specifically, two floating lidars were deployed off the coast of New Jersey by the New York State Energy Research and Development Authority (NYSERDA) in August and September 2019 (see Figure 2). Data are released publicly and in near real time [4] as 10-minute averages and from 20 to 200 m above water level in 20-m increments.

As will be made clear in Section 2.3, these Atlantic lidar data become critical in validating the Outer Continental Shelf WRF runs.

2.3 Validation Approach

Validation of the different WRF model setups is performed on diurnal, hourly, and annual scales. We consider three main metrics to assess model performance:

1. **Unbiased root-mean-square error (RMSE)**: Useful for separating out the bias contribution to the overall error and focusing only on the error as a result of model variability
2. **Bias**: Useful for analyzing the offset between model and observations and the extent to which the wind resource is underpredicted or overpredicted
3. **Earth mover's distance (EMD)**: Recently popularized for wind energy in the making of NEWA (Hahmann et al. 2020), the EMD (also called the Wasserstein distance) is a measure of the difference between two distributions. Specifically, the metric is equal to the area between two cumulative distribution functions and can

[4] https://oswbuoysny.resourcepanorama.dnvgl.com/

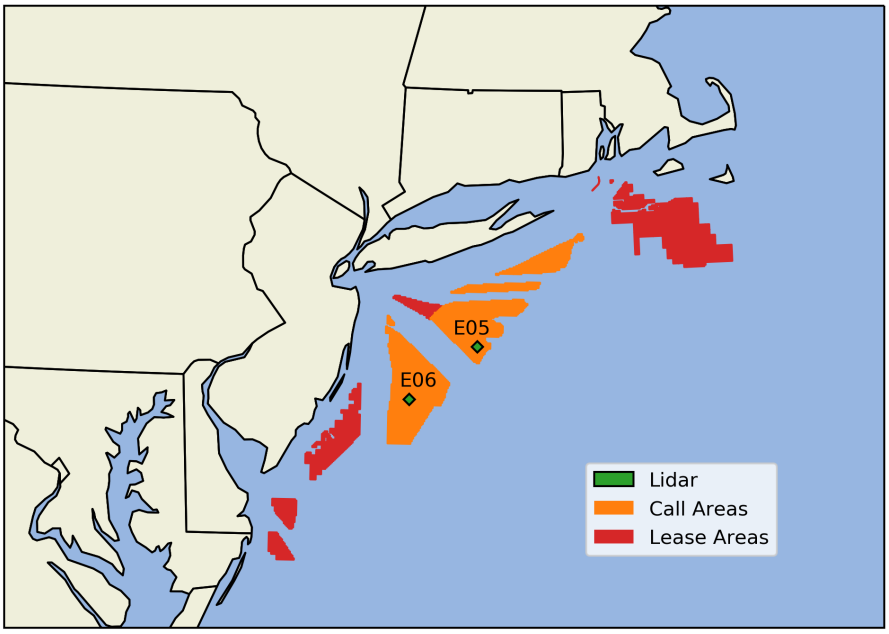

Figure 2. Locations of the NYSERDA-deployed floating lidars in current Atlantic wind energy Lease and Call Areas

be interpreted as the amount of "dirt" needed to move from one probability distribution (or pile) to another to make them equal. The key advantage of the EMD metric is that it accounts for cases where two distributions may have the same bias but have different shapes, as shown in Figure 3.

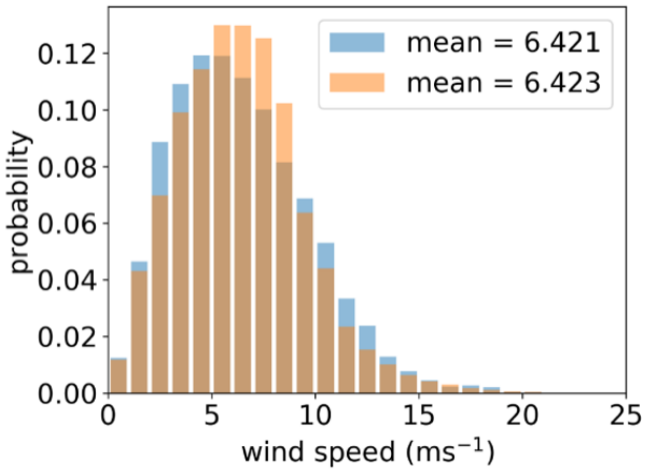

Figure 3. A comparison of two sample wind speed distributions, taken from Hahmann et al. 2020. The two distributions have the same mean but different shapes, which the EMD metric is able to quantify.

As shown in Table 3, validation was performed at the measurement heights of each observation station rather than at a fixed height relevant to wind energy (e.g., 100 m). For the buoys in particular, which have measurement heights near 4 m, NREL determined that the extrapolation of these wind speed measurements to a typical hub height, regard-

less of extrapolation method, would be associated with a prohibitively large uncertainty and would hinder a confident validation of different mesoscale model setups.

Instead, the modeled 10-m winds (which output from WRF as diagnostic variables) are interpolated to the buoy heights using the logarithmic wind speed profile:

$$U_{z_2} = U_{z_1} \frac{ln\left(\frac{z_2}{z_0}\right) - \psi\left(\frac{z_2}{L}, \frac{z_0}{L}\right)}{ln\left(\frac{z_1}{z_0}\right) - \psi\left(\frac{z_1}{L}, \frac{z_0}{L}\right)} \tag{2.1}$$

where U is wind speed, z_2 and z_1 are heights above the surface, z_0 is the roughness length, ψ is the stability function, and L is the Obukhov length. The stability functions from Jiménez et al. 2012 are used, which are the same used by WRF to diagnose the 10-m wind speed from model-level wind speeds.

To interpolate model results to the radar and lidar measurement heights, a basic linear interpolation of wind speeds in the neighboring model levels is performed. We can justify basic linear interpolation based on the high vertical resolution of the WRF model near the surface (see Table 2), where the wind profile between model levels can reasonably be approximated as linear over a short distance.

2.4 Validation Results

In this section, we present the results of the WRF model setup validation. Throughout this section, the different ensemble members are labeled using the following nomenclature: *'<Reanalysis product>_<SST Product>_<PBL scheme>_<LSM>.'*

2.4.1 Hourly Data

First, we present performance metrics for the hourly data in Figures 4–6 averaged across all sites. Performance metrics on a site-by-site basis are provided in the Appendix. Figure 4 shows that model setups using ERA5 as a large-scale forcing have about 0.2 m·s^{-1} or 10% lower RMSE than those that use MERRA-2, while model setups using the YSU PBL scheme have a 0.1 m·s^{-1} or 5% lower error than those that use the MYNN PBL scheme. The SST product and LSM choice have a relatively negligible impact.

Figure 5 shows the least bias for model setups using ERA5 as a forcing product, MYNN as the PBL scheme, and Noah as the LSM model. In fact, bias is nearly half compared to models using MERRA-2, the YSU PBL scheme, and the Noah-MP LSM. The SST product has a relatively negligible impact.

Figure 6 shows the least EMD for model setups using ERA5 as a forcing product, MYNN as the PBL scheme, and Noah as the LSM model. Again, the SST product has a relatively negligible impact.

2.4.2 Diurnal Analysis

In this section, we assess the performance of each model in its representation of the diurnal cycle. Model performance is assessed as an average across all sites. Wind speeds are normalized by their respective mean wind speed over the diurnal period to remove model biases and focus only on the variability of diurnal trends.

Figure 7 shows the mean diurnal cycle across all measurement sites. The observed diurnal trend reaches a peak of about 11% above its mean value around 18:00 PST and a minimum about 10% below its mean value at around 10:00 PST. Most models represent the variability of the diurnal cycle well. However, model setups using the MERRA-2 reanalysis and its default OSTIA sea-surface temperature product tend to overestimate the magnitude of the diurnal cycle. This performance is likely related to the role of SST in the coastal diurnal cycle and the coarse resolution of the MERRA-2 model (0.5 x 0.65 degrees). It is likely that this coarse resolution is unable to capture the horizontal distribution of SST in active upwelling areas, thus affecting the accurate modeling of the diurnal cycle.

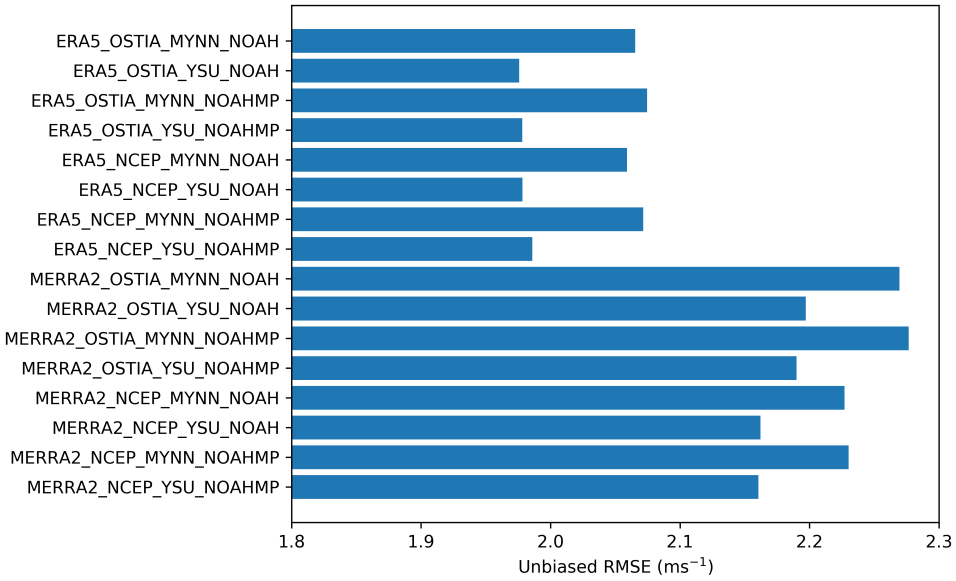

Figure 4. Mean unbiased RMSE in modeled wind speeds at validation measurement heights, averaged across all sites. Note that the origin does not start at zero.

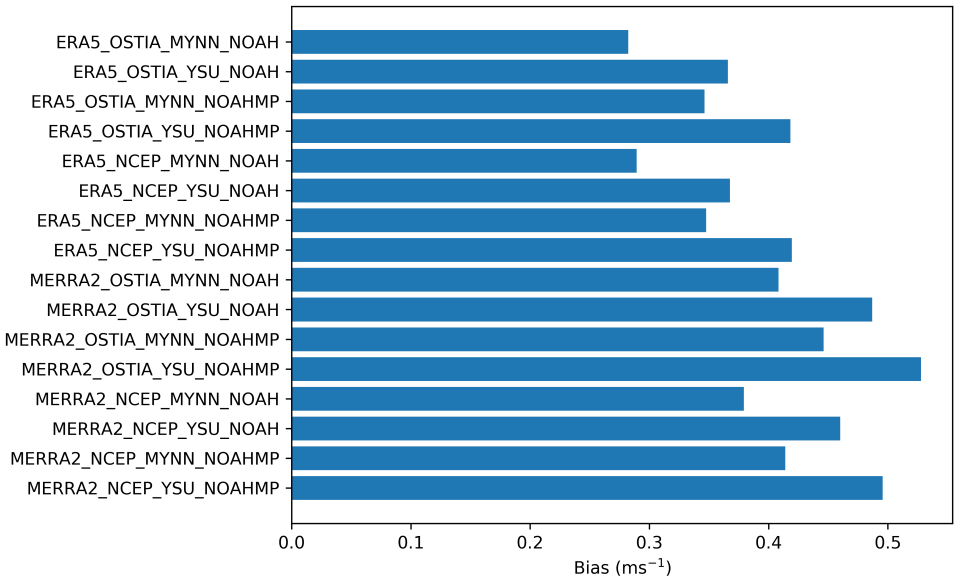

Figure 5. Mean bias in modeled wind speeds at validation measurement heights, averaged across all sites

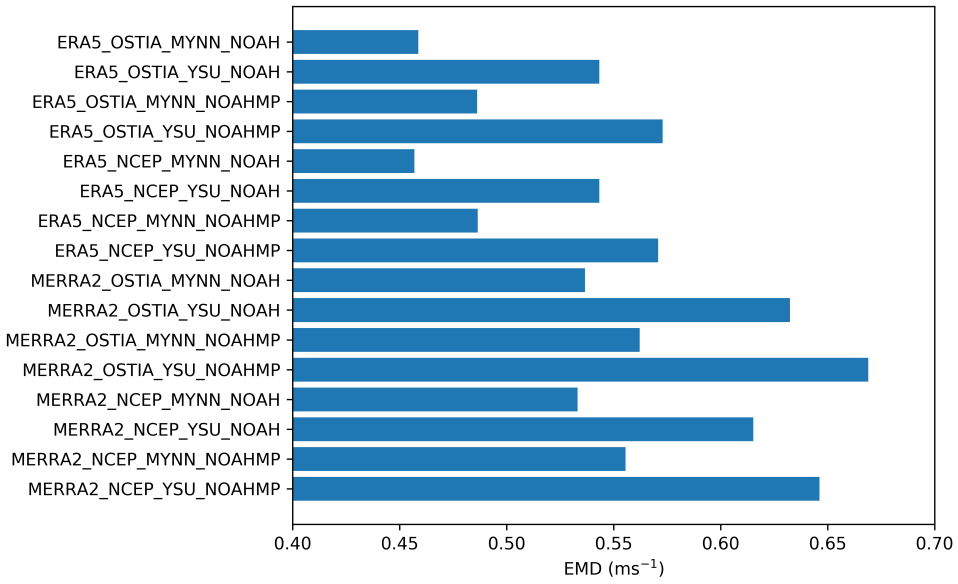

Figure 6. Mean EMD in modeled wind speeds at validation measurement heights, averaged across all sites. Note that the origin does not start at zero.

The mean RMSE across the 24-hour cycle in Figure 7 is summarized in Figure 8. Again, models using ERA5 as large-scale forcing tend to have the lowest RMSE across the diurnal cycle. Models using the YSU planetary boundary layer scheme combined with the Noah-MP LSM tend to have the lowest RMSE.

2.4.3 Wind Profiles

In this section, we examine modeled wind profiles at the buoys closest to the wind energy Call Areas. No observed data up to hub height are available to validate the modeled wind profiles; rather, the focus is on exploring wind profile sensitivity to the different model setups.

Figure 9 shows the annual average wind profiles up to 200 m at Buoys 46022 and 46028, which are adjacent to the Humboldt and Morro Bay Call Areas, respectively. We focus here on distinguishing only the PBL schemes as different colors, given the clear separation of wind profiles based on which PBL scheme is used. Near Humboldt, wind profiles based on the YSU scheme tend to model wind speeds 100 m and above about 1 m·s^{-1} lower than those modeled using MYNN. A similar mean difference is found at Morro Bay but with more spread in the submembers. This difference in 100-m wind speeds is driven by the tendency for the MYNN scheme to model much higher wind shear below 50 m relative to the YSU scheme. Above 50 m, wind shear is comparable between the two PBL schemes.

2.5 Stability Analysis and PBL Schemes

As illustrated in Figure 9, the implications of choosing MYNN or YSU for the new 20-year data set will have significant implications for OCS resource and energy modeling. Therefore, further validation is performed between these two PBL schemes. Focusing only on the two WRF setups that use the ERA5 reanalysis, OSTIA sea-surface temperature and Noah MP (all of which validated best in Section 2.4), we explore PBL sensitivity in Table 4. Here, the mean values of the three performance metrics across all observation stations are summarized. The table shows that YSU has lower unbiased RMSE, whereas MYNN has lower absolute bias and EMD.

To better understand the differences in modeled wind profiles between the MYNN- and YSU-based WRF runs, an

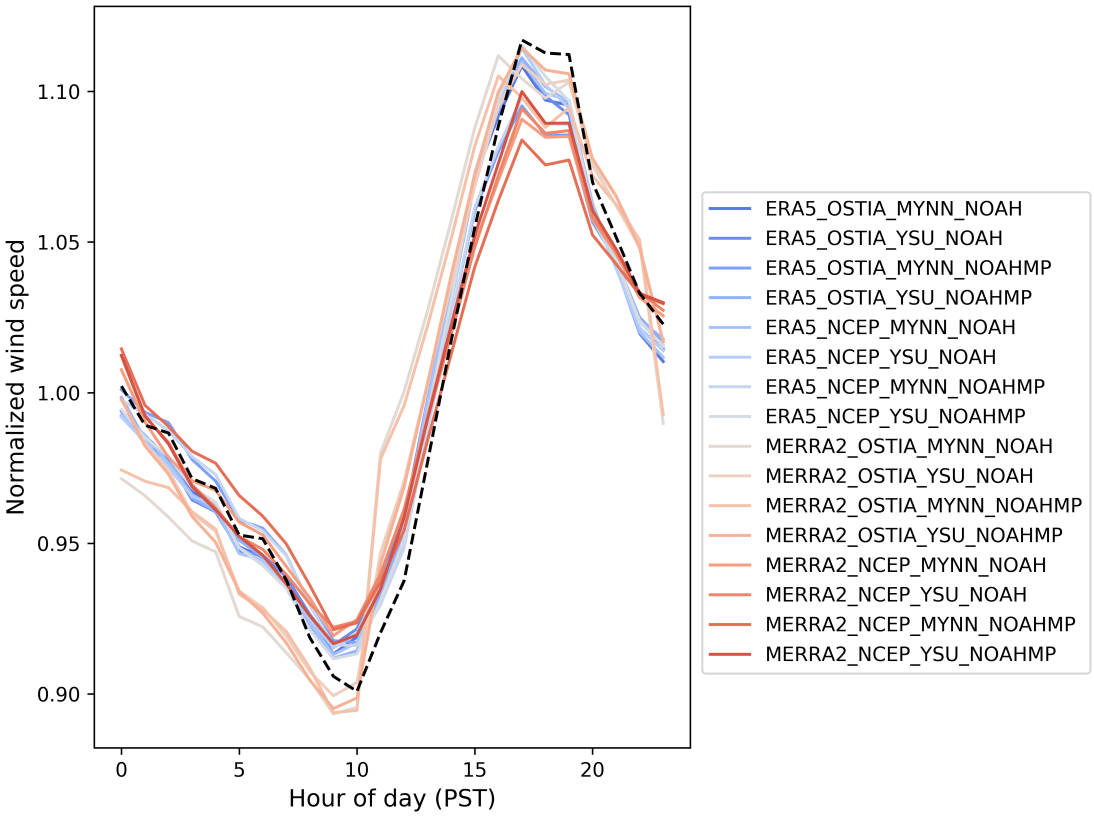

Figure 7. Mean diurnal cycle of modeled wind speeds from the different ensembles, normalized to the mean wind speed and averaged across all observations stations. The dashed black line denotes the observations.

Table 4. Mean Performance Metrics for MYNN- and YSU-Based Simulations Across All Observation Stations

Metric	MYNN	YSU
Unbiased RMSE ($m \cdot s^{-1}$)	2.07	1.98
Bias ($m \cdot s^{-1}$)	0.28	0.36
EMD ($m \cdot s^{-1}$)	0.46	0.54

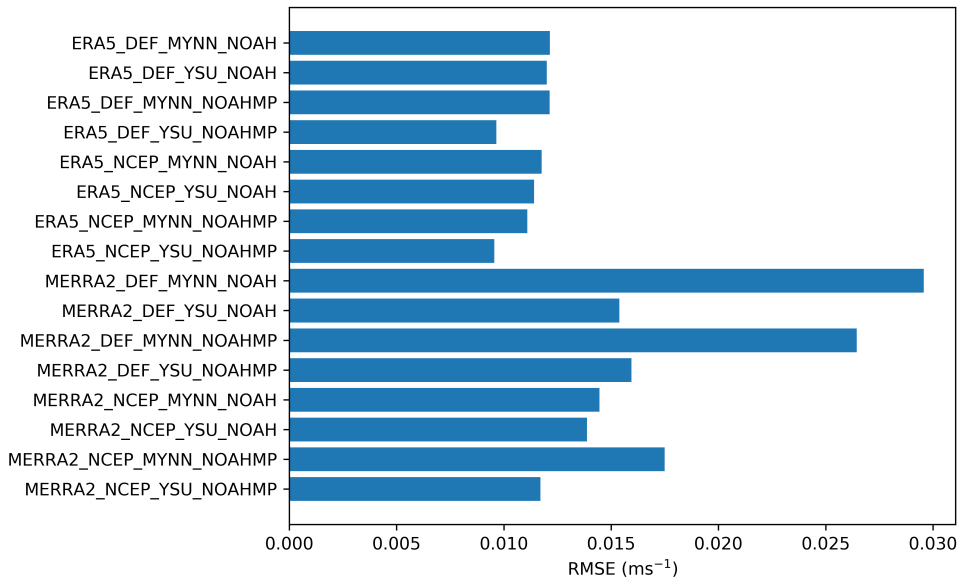

Figure 8. RMSE of normalized diurnal winds for the different WRF ensembles, averaged across all observation stations

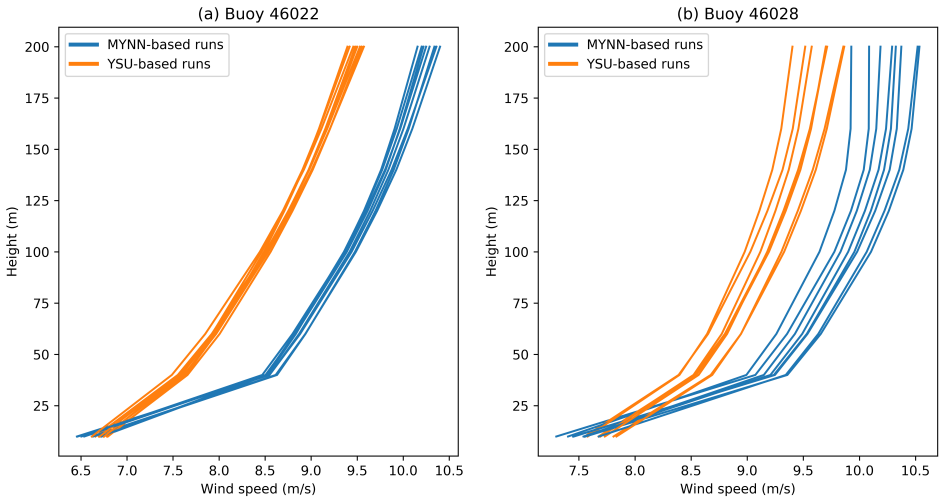

Figure 9. Mean modeled wind profiles at Buoy 46022 (a) and Buoy 46028 (b), which are adjacent to the Humboldt and Morro Bay Call Areas, respectively. MYNN-based profiles are in blue and YSU-based profiles are in orange.

analysis of PBL schemes in different atmospheric stability conditions is required.[5] There are various metrics used to quantify atmospheric stability in the lower part of the atmosphere. Here, we use the bulk Richardson number, Ri_B, which is a combined measure of wind shear and temperature shear between two vertical layers:

$$Ri_B = \frac{g}{\theta_v} \frac{\Delta z \Delta \theta_v}{(\Delta U)^2 + (\Delta V)^2} \tag{2.2}$$

where g is gravitational acceleration, θ_v is absolute virtual potential temperature, $\Delta\theta_v$ is the virtual potential temperature difference across a layer of thickness Δz, and ΔU and ΔV are the changes in horizontal wind components across that same layer. Values of $Ri_B < 0$ represent thermodynamically unstable conditions and $Ri_B > 0$ represent stable conditions, with instability or stability increasing monotonically with the magnitude of Ri_B. For neutral conditions, $Ri_B \approx 0$.

We calculate Ri_B between 200 m and the surface and compare the frequency of different stability regimes using Ri_B in OCS in Figure 10 over the 2017 validation year. We contrast both the MYNN and YSU schemes directly by using the same reanalysis product (ERA5), SST product (OSTIA), and LSM (Noah). We categorize stability regimes based on the Ri_B thresholds listed in Table 5, adapted from Kalverla et al. 2020 to include six stability categories ranging from very unstable to very stable conditions.

Table 5. Stability Regimes Used in This Study, Based on the Bulk Richardson Number Between 200 m and the Surface

Stability Regime	Ri_B Range
Very unstable	$Ri_B \leq -0.1$
Unstable	$-0.1 < Ri_B \leq -0.025$
Weakly unstable	$-0.025 < Ri_B \leq -0$
Weakly stable	$0 < Ri_B \leq 0.025$
Stable	$0.025 < Ri_B \leq 0.1$
Very stable	$Ri_B > 0.1$

A breakdown of stability regimes by percentage frequency across the OCS is shown in Figure 10. Both the MYNN and YSU schemes model predominately weakly unstable and weakly stable conditions across the whole OCS out to the 200-nautical-mile Exclusive Economic Zone. However, YSU tends to model very unstable to unstable conditions more frequently than MYNN, with the opposite true for weakly stable through very stable conditions. Focusing on the locations of the wind energy Call Areas, the bottom row reveals that both PBL schemes estimate very stable conditions close to the coastline, which reflects strong upwelling of cold seawater to the surface, inducing a stable stratification in the lower atmosphere. In these areas, the MYNN scheme is considerably more likely to model very stable conditions than the YSU scheme. It is likely that there is seasonal dependence in stability conditions (e.g., warmer air or a colder sea would favor stable conditions); however, a seasonal analysis is beyond the scope of the present study.

The impact of these stability regimes on hub-height wind speeds is illustrated in Figure 11. Here, we compare the mean 100-m wind speeds in 2017 across the OCS between MYNN and YSU in the different stability regimes. The top row in Figure 11 shows weak mean-modeled 100-m winds in very unstable conditions that would produce little power. In unstable to weakly unstable conditions, YSU models slightly higher wind speeds. From weakly stable to stable conditions, we observe a significant increase in mean 100-m winds in MYNN than YSU, particularly close to the coast and at the current wind energy Call Areas. At some locations, the mean annual wind speed difference

[5]Unstable conditions usually occur when warm air sits underneath colder air (e.g., during strong surface heating in summer). The lower density of the warmer air causes it to rise above the cold air, inducing strong vertical mixing of momentum and leading to wind profiles that are relatively constant with height. By contrast, stable conditions occur when colder air sits underneath warmer air (e.g., during surface cooling at night). The higher density of the underlying colder air suppresses turbulent vertical mixing and produces wind profiles with strong wind shear.

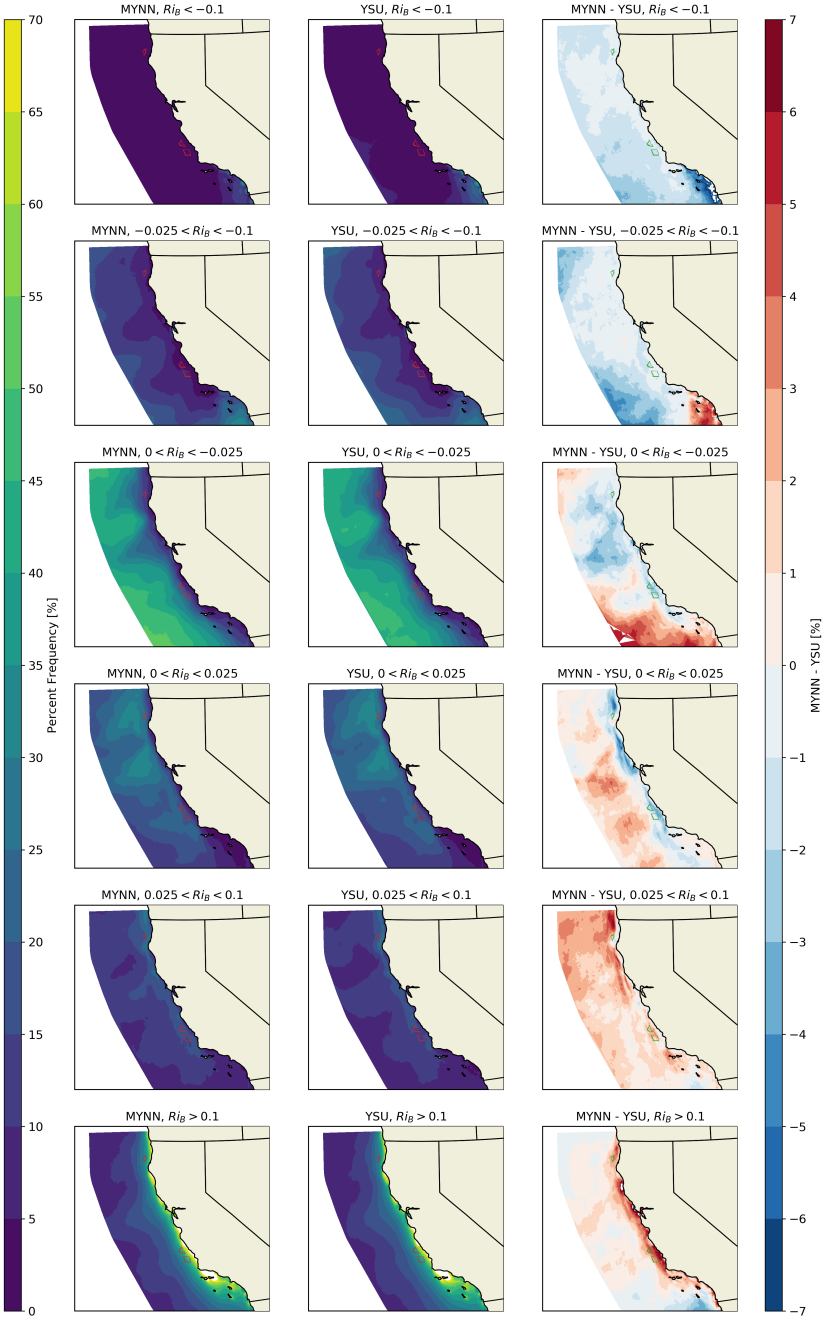

Figure 10. Percentage breakdown of atmospheric stability regimes across the OCS between the MYNN PBL scheme (left column) and the YSU scheme (middle column). The difference in frequencies is shown in the rightmost column.

exceeds 2 m·s^{-1}. Based on this map, it appears that the divergence of MYNN- and YSU-based wind profiles as shown at Buoys 46022 and 46028 is driven by this divergence in weakly stable to stable conditions.

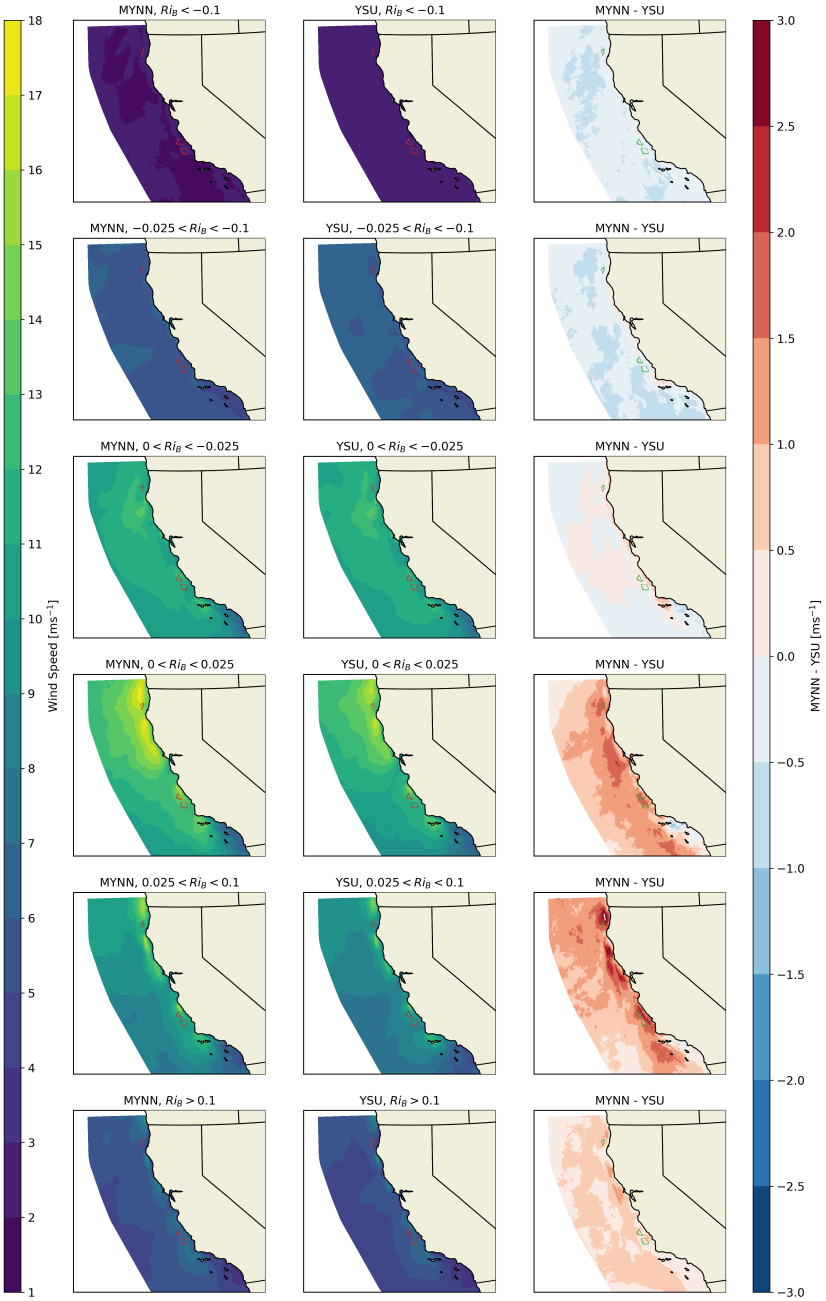

Figure 11. Mean 100-m wind speeds in each stability regime across the OCS for the MYNN PBL scheme (left column) and the YSU scheme (middle column). The difference between the two PBL schemes is shown in the rightmost column.

We can explore this difference in more detail at these buoys by examining wind profiles by stability regime in Figure 12. Here, we focus on Buoy 46022 (i.e., at the Humboldt Call Area). As suspected, the figure shows close agreement between the two PBL schemes from unstable to weakly stable conditions, but strong divergence in weakly stable to

stable conditions. Most of this divergence occurs in the lower 50 m of the atmosphere, where the MYNN scheme shows a considerably sharper gradient before both PBL schemes model similar wind shear up to 200 m. Finally, we note that Humboldt is subject to some form of stable atmospheric conditions most of the time (81.9%) according to the Ri_B values. Therefore, the mean modeled wind profiles in OCS Call Areas are strongly influenced by how the PBL scheme performs under such conditions.

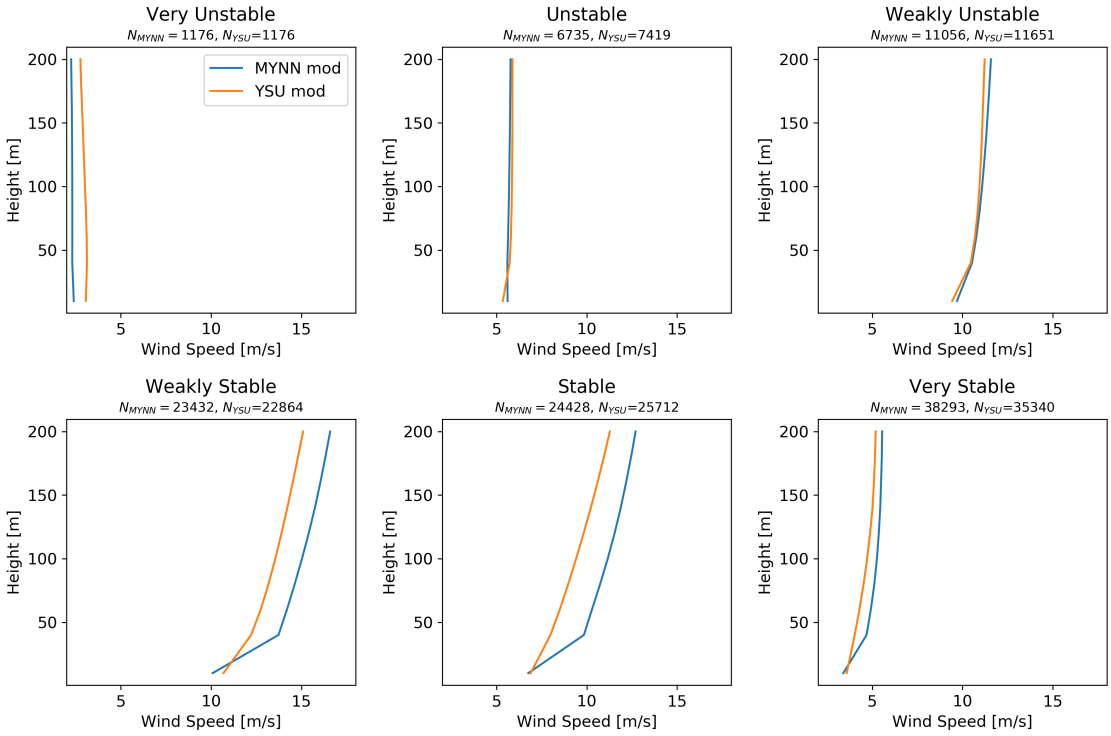

Figure 12. Mean modeled wind profiles at Buoy 46022 (Humboldt Call Area) by stability regime for the MYNN-based (blue) and YSU-based (orange) WRF setups

The lack of observations available to validate these divergent wind profiles is a significant limitation to this analysis. Specifically, a floating lidar measuring offshore wind profiles near these wind energy Call Areas is crucial to determine which of these PBL schemes is best suited for accurate wind modeling in the OCS.

2.5.1 Leveraging Atlantic Lidars

Lacking floating lidar to validate the modeled wind profiles in the OCS, we instead leverage recently deployed floating lidars in the Atlantic via NYSERDA (see Section 2.2.1).

An exhaustive analysis of the 16 WRF model setups at these lidar locations is beyond the scope of this study. Instead, we compare only the MYNN and YSU planetary boundary layer schemes to determine which is most accurate across the different stability regimes. For this analysis, we use the ERA5 reanalysis, the OSTIA sea-surface temperature product, and the Noah land surface model, which validated best against the OCS observations. We run the same WRF setup described in Section 2.2 from August 2019 to May 2020 over a domain centered on the two lidars.

Mean modeled and observed wind profiles at each lidar location are shown in Figure 13. Both the MYNN- and YSU-modeled profiles overestimate wind shear at lower heights and underestimate shear at upper heights. There is relatively little difference between the mean modeled profiles apart from higher shear observed with the MYNN profile at lower heights. These similar profiles are in contrast to the mean profiles observed in the OCS (Figure 9).

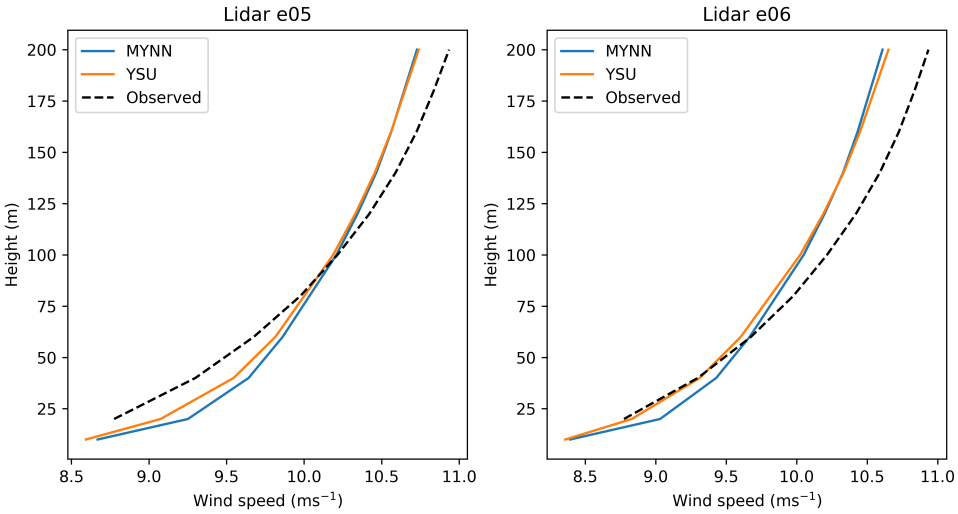

Figure 13. Mean modeled and observed wind profiles at NY-SERDA floating Lidar E05 from September 2019 through May 2020

Similar to Figure 12, we separate wind profiles at Lidar E05 into stability regimes according to the modeled bulk Richardson number between 200 m and the surface, as modeled from the MYNN-based run. Results are shown in Figure 14, and we note that similar results were found at Lidar E06 and therefore not shown here. Similar to the OCS (Figure 12), the winds at Lidar E05 are weaker in unstable conditions and very unstable conditions, and stronger from weakly unstable through stable conditions. The modeled profiles also show similar relative behavior to the OCS: they are similar from very unstable to weakly unstable conditions before diverging in weakly stable to stable conditions, with higher winds modeled using the MYNN scheme. Compared to the observations, there is no clear improvement in one modeled profile over another. Focusing on weakly stable and stable conditions where the modeled profiles differ the most, Figure 14 indicates better performance with YSU in weakly stable conditions and with MYNN in stable conditions.

Focusing on the 100-m wind speeds, we present performance metrics for the MYNN- and YSU-based profiles, averaged across both lidars, in Figure 15. The YSU model has slightly lower unbiased RMSE in most stability regimes, apart from very unstable and very stable conditions. The YSU model generally has lower bias in the unstable regimes, whereas the MYNN model has lower bias in the stable regimes. Modeled performance in EMD is similar to that of the bias metric. Overall, neither the MYNN nor YSU model is showing a clear improvement over the other.

Given the predominance of stable conditions in the OCS, the relative performance of the MYNN- and YSU-based simulations at the NYSERDA lidars should be more weighted toward performance in stable conditions. To do so, we multiply the performance metrics in each stability regime in Figure 15 by the mean percentage frequency of that stability regime across the three Call Areas. By taking the sum across all weighted stability regimes, we can assess how well the MYNN- and YSU-based simulations might perform in the OCS had floating lidar data been available. Results are summarized in Table 6 and Figure 16.

The weighted results show that the MYNN and YSU performances are very similar: YSU-based simulations have slightly less unbiased RMSE overall, whereas MYNN-based simulations have moderately lower bias and slightly lower EMD overall.

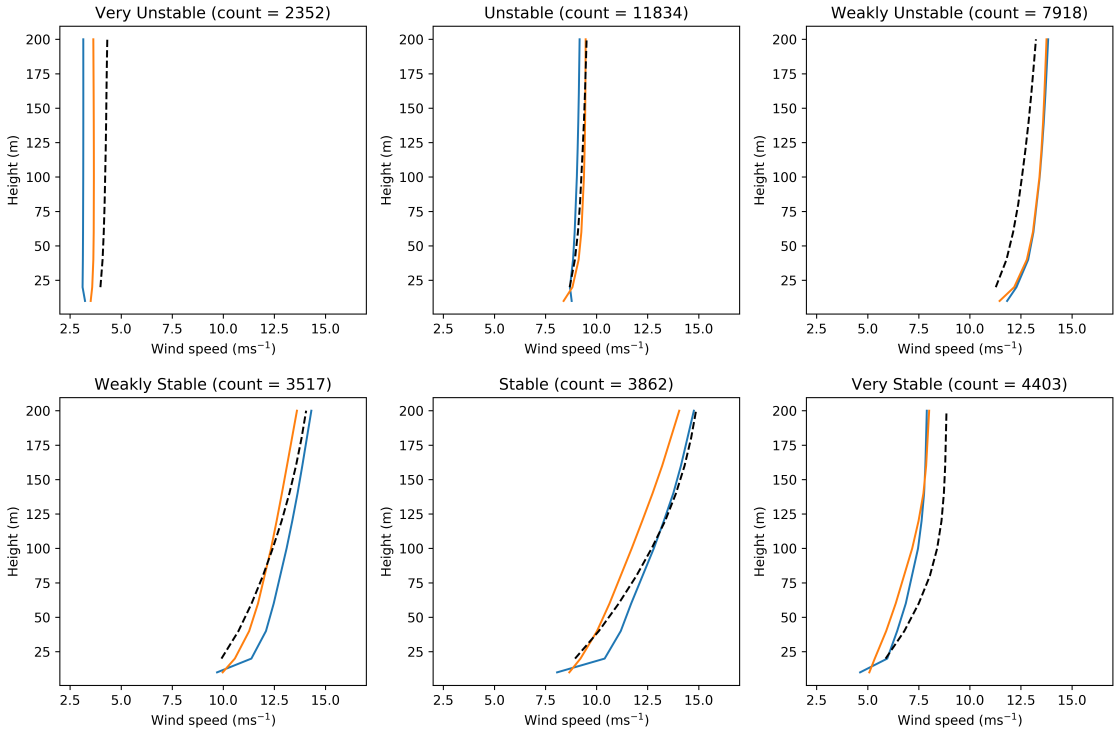

Figure 14. Mean modeled wind profiles at NYSERDA floating lidars, taken as an average between E05 and E06. MYNN profiles are in blue, YSU in orange, and observed in dotted black.

Table 6. Performance Metrics for MYNN- and YSU-Modeled 100-m Wind Speeds, Averaged Across Both the E05 and E06 NYSERDA Floating Lidars and Weighted by Frequency of Stability Regimes Across the Three California Call Areas

Stability Regime	Frequency at Humboldt (%)	Unbiased RMSE (m·s^{-1})		Bias (m·s^{-1})		EMD (m·s^{-1})	
		MYNN	YSU	MYNN	YSU	MYNN	YSU
Very unstable	1.1	1.57	1.57	-1.04	-0.47	1.04	0.47
Unstable	6.4	1.90	1.83	-0.34	0.02	0.47	0.25
Weakly unstable	10.5	2.27	2.24	0.67	0.66	0.67	0.67
Weakly stable	22.3	2.53	2.30	0.62	-0.10	0.68	0.31
Stable	23.2	2.87	2.80	0.07	-0.91	0.51	0.94
Very stable	36.4	2.79	2.82	-1.00	-1.12	1.01	1.12
	Weighted total	**2.62**	**2.56**	**0.63**	**0.72**	**0.75**	**0.79**

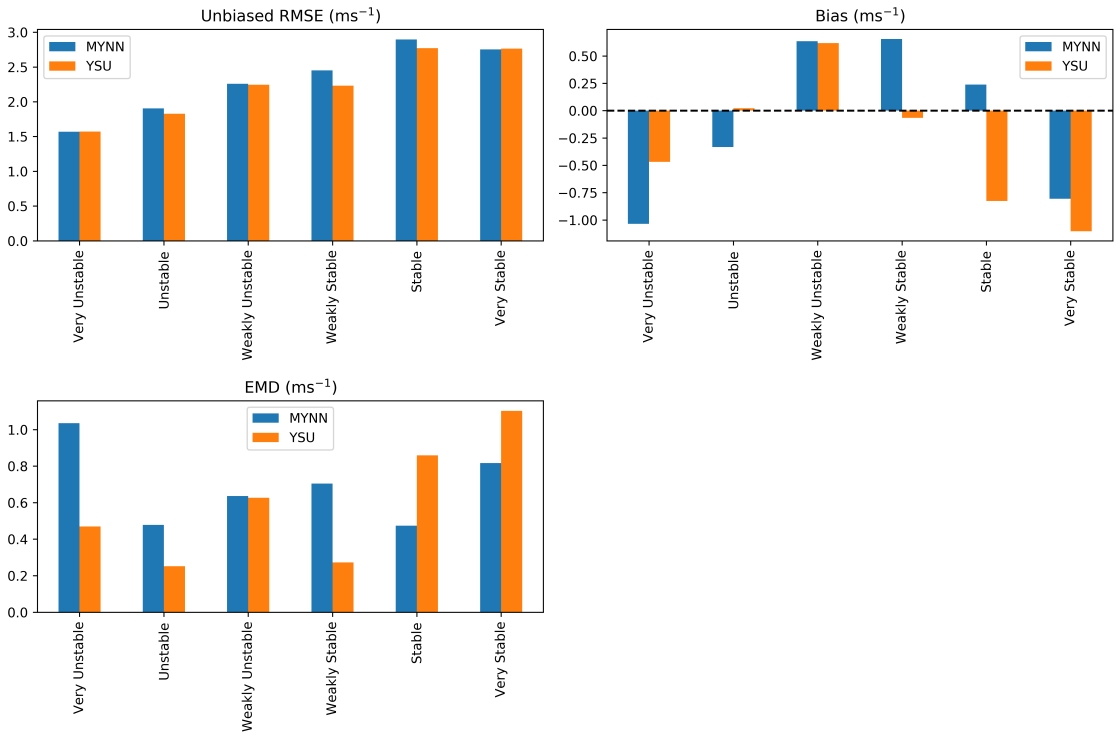

Figure 15. Performance metrics for MYNN- and YSU-modeled 100-m wind speeds, averaged across both the E05 and E06 NYSERDA floating lidars

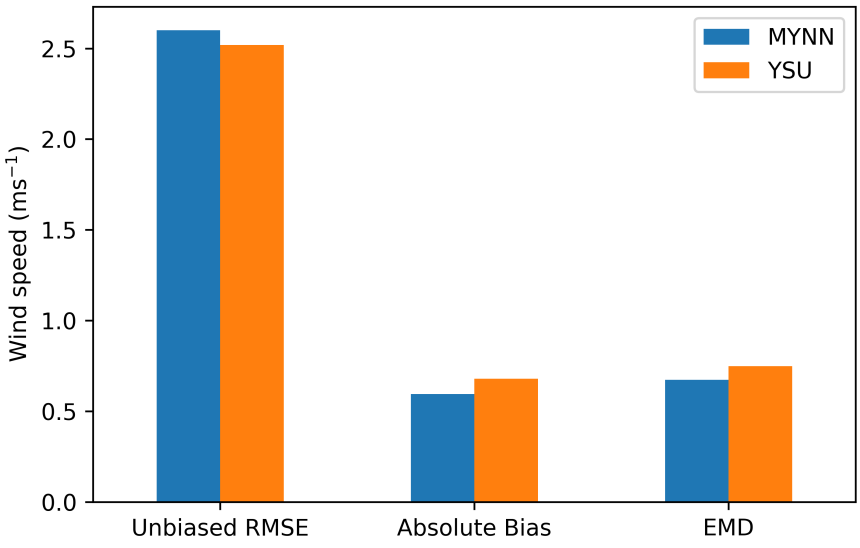

Figure 16. Performance metrics for MYNN- and YSU-modeled 100-m wind speeds, averaged across both the E05 and E06 NYSERDA floating lidars and weighted by frequency of stability regimes at the Humboldt Call Area in California

2.6 Final Choice on 20-Year Model Setup

In this section, we present a comparison of 16 WRF model setups to be considered as the final model setup in which to run the updated 20-year wind resource analysis for the OCS. These simulations were compared against buoy and coastal radar measurements in California, as well as two floating lidars in the Atlantic off the coast of New Jersey.

Based on the analysis of buoy and coastal radar measurements in the OCS, we found that:

1. WRF models forced using the ERA5 reanalysis product had lower unbiased RMSE, bias, and EMD than those forced by the MERRA-2 reanalysis product
2. The impact of SST product was less significant, with the OSTIA product generally showing slightly better performance
3. The impact of LSM was not significant.

These results justify the choice of the ERA5 reanalysis, OSTIA SST, and the Noah LSM scheme for use in the 20-year simulations.

The choice between MYNN and YSU is more challenging given how similar they performed against observations. However, the MYNN PBL scheme slightly outperformed YSU overall in the following ways:

1. Moderately lower bias and EMD than YSU when evaluated at the California buoys and radars
2. Moderately lower bias and slightly lower EMD than YSU when evaluated at the NYSERDA floating lidars and weighted based on the frequency of stability regimes across the three Call Areas.

Furthermore, as described in Section 2.1, the MYNN scheme continues to be the focus of significant R&D and is used in most other operational NWP products and wind atlases. Therefore, there is a precedent in the atmospheric community toward aligning with the use of MYNN.

Table 7. Final WRF Component Selection for New 20-Year Wind Resource Data Set for the OCS

Model Component	Selection for New 20-Year Data Set
Reanalysis product	ERA5
PBL scheme	MYNN
SST product	OSTIA
LSM	Noah

3 CA20 Final Data Set

3.1 Updated Wind Resource Maps

Using the final WRF setup summarized in Table 7, the updated annual 100-m wind resource maps for the OCS are shown in Figures 17, 18, and 19 for all of OCS, Northern California, and Southern California, respectively.

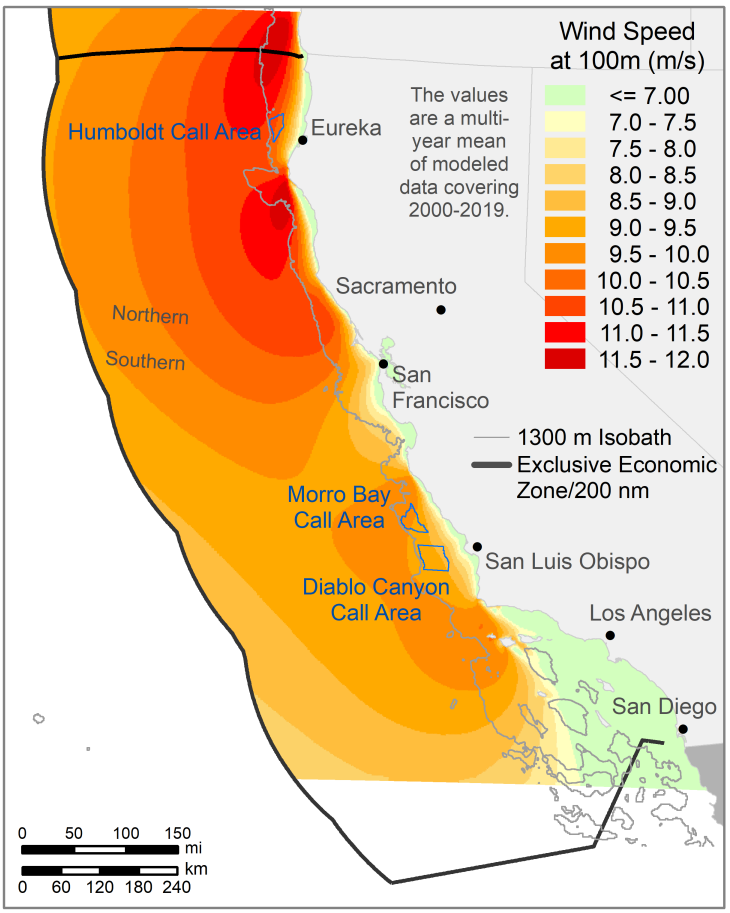

Figure 17. Mean annual wind resource for the OCS based on the new 20-year data set

3.2 Update to Technical Potential

The resource assessment using the CA20 wind resource data indicates an increase in technical potential for the OCS, summarized in Table 8. This increase in technical potential is based on comparisons with NREL's 2016 U.S. wind energy resource assessment, which was largely based on an AWS Truepower data set (Musial et al. 2016) and comparisons with the NREL WTK data. In NREL's 2016 resource assessment (Musial et al. 2016), the technical potential included the offshore wind capacity that could be developed while taking into account exclusion factors related to water depth (1,000 m), mean wind speed (greater than 7 $m \cdot s^{-1}$), and reductions due to possible conflicting uses and environmental conflicts (a total of 150 GW). By contrast, gross potential is the capacity without these filters.

In this new CA20 resource assessment, the technical potential increases to 201 GW. This is due to three factors:

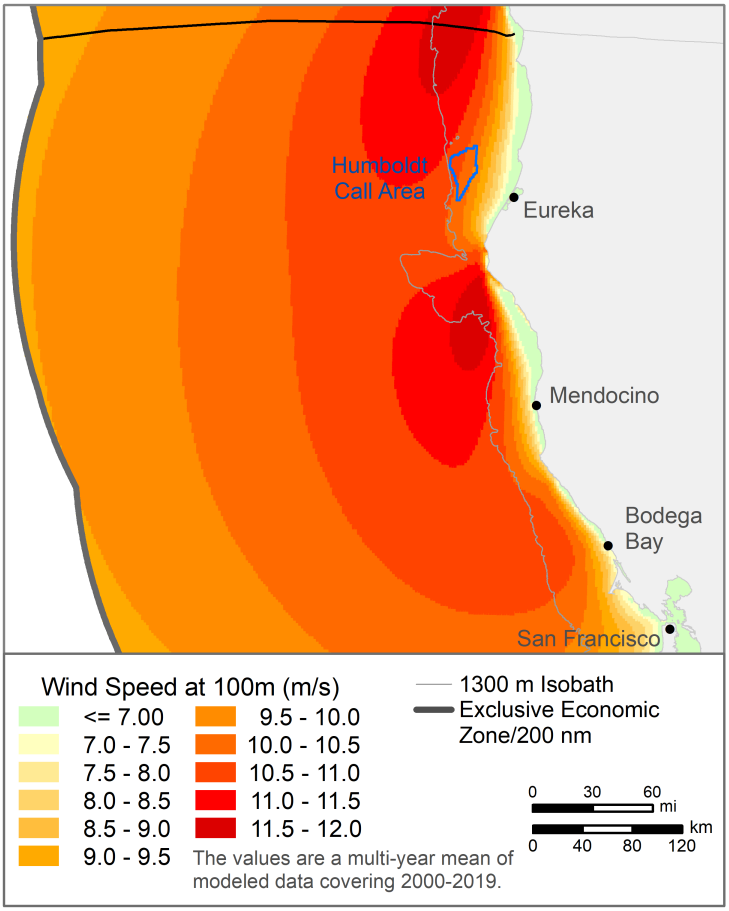

Figure 18. Mean annual wind resource for the OCS based on the new 20-year data set, focused on Northern California

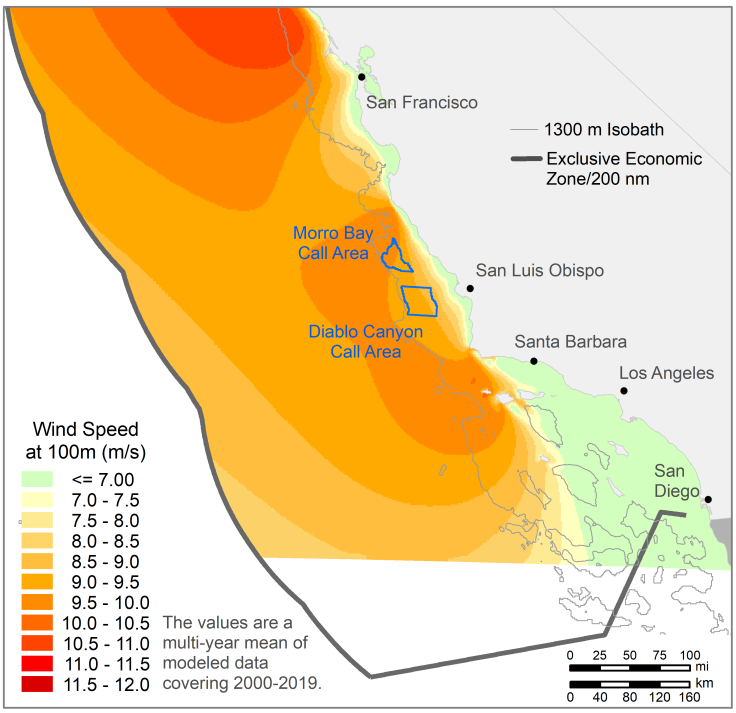

Figure 19. Mean annual wind resource for the OCS based on the new 20-year data set, focused on Southern California

1. In the 2016 assessment, a significant reduction was taken on the technical resource to account for possible competing uses and environmental exclusions. In this CA20 assessment, these exclusions were not taken, which makes the total technical potential significantly higher. The 2016 exclusions, based on percentages of the resource area, were based on national estimates and did not reflect a careful marine spatial planning process for California. Therefore, the CA20 assessment does not try to account for any possible competing uses or environmental reductions. This task is left to state and federal planning agencies.
2. We have increased the depth limit from 1,000 m to 1,300 m for floating wind installations (Figure 20, with bathymetry data provided by NOAA's Coastal Relief Model), which reflects potential advancements in floating wind mooring technologies. This new depth limit resulted in some additional resource area, mostly on the western boundary. We do not explicitly calculate the increase in technical potential as a result of the increased depth limit, but it is expected to be minor compared to the impact from exclusion adjustments, as described in the previous point.
3. The 7-m·s^{-1} wind speed low-wind filter remained the same, but because of some modeled increases in the annual average wind speeds in the CA20 data set, the resource area expanded and pushed the southern boundary slightly outward. We calculated this increased wind resource capacity caused by higher average wind speeds in the CA20 assessment to be 4.7% compared to the 2016 assessment.

Breakdowns of technical potential by wind speed bins, distance to shore, and water depth are shown in Tables 9, 10, and 11, respectively.

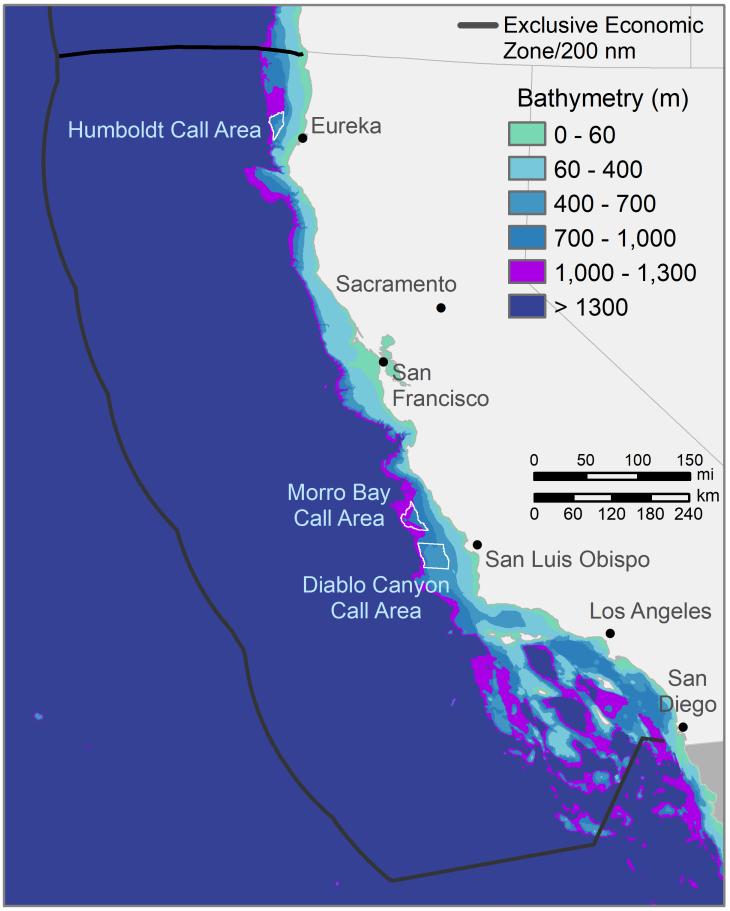

Figure 20. Bathymetry of the OCS up to 1,300 m

Table 8. Comparison of Technical Potential Estimates from 2016 Report and This Report

Metric	2016 Report	This Report	
		WIND Toolkit	CA20 Data Set
Minimum average wind speed ($m \cdot s^{-1}$)	7.0	7.0	7.0
Maximum water depth (m)	1,000	1,300	1,300
Array density ($MW \cdot km^{-2}$)	3.0	3.0	3.0
Gross potential (km^2)	566,058	566,058	566,058
Gross potential (GW)	1,698	1,698	1,698
Technical potential (km^2)	49,916	64,048	67,067
Technical potential (GW)	150	192	201

Table 9. Technical Potential Estimates from CA20 Data Set by Wind Speed Bins. Northern and Southern Potentials are Split Based on a Line at 37.8^o, Which Runs Through San Francisco.

Bin ($m \cdot s^{-1}$)	Northern CA (MW)	Southern CA (MW)	Total (MW)
7.0–7.5	2,845	14,636	17,480
7.5–8.0	3,086	16,106	19,192
8.0–8.5	3,540	19,787	23,327
8.5–9.0	4,233	21,388	25,621
9.0–9.5	5,313	33,465	38,778
9.5–10.0	6,972	26,836	33,808
10.0–10.5	12,268	549	12,817
10.5–11.0	15,540	0	15,540
11.0–11.5	8,404	0	8,404
11.5–12.0	6,234	0	6,234
Total	68,435	132,767	201,202

Table 10. Technical Potential Estimates from CA20 Data Set by Distance to Shore. Northern and Southern Potentials are Split Based on a Line at 37.8^o, Which Runs Through San Francisco.

Bin (Nautical Miles)	Northern CA (MW)	Southern CA (MW)	Total (MW)
<3	6,643	9,094	15,737
3–15	36,364	53,143	89,507
>15	25,428	70,530	95,958
Total	68,435	132,767	201,202

Table 11. Technical Potential Estimates from CA20 Data Set by Water Depth. Northern and Southern Potentials are Split Based on a Line at 37.8^o, Which Runs Through San Francisco.

Bin (m)	Northern CA (MW)	Southern CA (MW)	Total (MW)
<60	6,317	6,907	13,224
60–400	27,533	34,227	61,761
400–700	9,620	31,612	41,232
700–1,000	12,969	27,740	40,709
1,000–1,300	11,996	32,280	44,276
Total	68,435	132,767	201,202

4 Comparison to WIND Toolkit

In this section, we compare the CA20 data set against the original WIND Toolkit. We focus mainly on changes to the annual wind resource, particularly at the wind energy call areas, and describe the cause for any changes.

Throughout this section, we refer to the original WIND Toolkit as WTK for brevity.

4.1 Summary of Changes in Wind Resource

In Figure 21, we compare the mean annual wind resource between CA20 and WTK. The rightmost figure shows the difference in annual 100-m wind speeds between the two data sets, with positive (red) values indicating a higher wind resource modeled using the new CA20 data set. We see significant increases in the wind resource across the OCS, especially near the coastline and at the wind energy call areas.

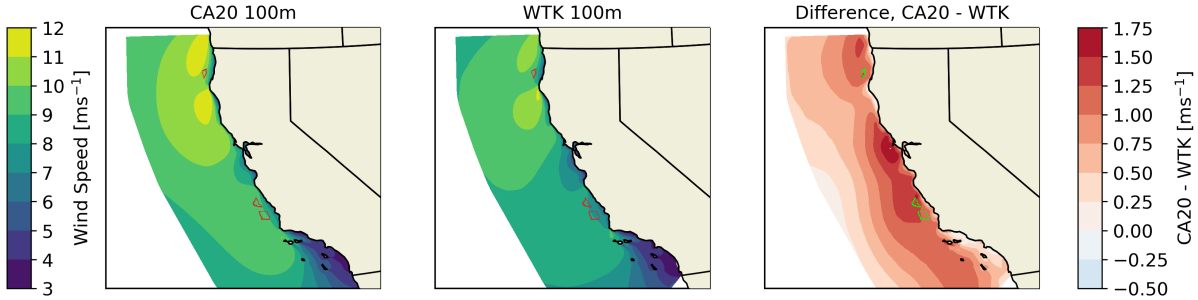

Figure 21. Mean 100-m wind speeds for the OCS modeled using CA20 (left) and WTK (middle). The difference between the two modeled data sets is shown on the right. Call areas are shown in red (left and center) and green (right).

Table 12 summarizes the change in mean annual 100-m wind resource at the centroids of each wind energy call area. The modeled mean wind speeds increase substantially at each call area with the CA20 data set: 10.6%, 16.1%, and 19.2% at Humboldt, Morro Bay, and Diablo Canyon, respectively.

Table 12. Comparison of Mean Annual 100-m Wind Speeds Between the WIND Toolkit and the New 20-Year Data Set at the Offshore California Call Area Centroids

Call Area	Mean Wind Speed (m·s^{-1})		Change	
	WIND Toolkit	Updated Data Set	(m·s^{-1})	(%)
Humboldt	9.41	10.41	1.00	10.6
Morro Bay	8.20	9.52	1.32	16.1
Diablo Canyon	7.70	9.18	1.48	19.2

These large increases in the wind resource will have important implications for the feasibility and competitiveness of the California offshore wind industry. Because of these implications, we explore in Section 4.2 the reasons for this increase and attribute it to the main differences in the CA20 and WTK model setups.

4.2 Explaining the Increased Wind Resource Estimates

To explain the substantial increase in the modeled wind resource with the new CA20 data set compared to the original WTK, we first highlight the main differences between the models. These differences are summarized in Table 13 and here:

- **Updated reanalysis product from ECMWF**: The ERA5 reanalysis, which replaces its predecessor ERA-interim, used in the WTK.
- **PBL scheme**: As described in Section 2, the choice of PBL scheme has significant impact on mean wind profiles in the OCS. The new CA20 model uses MYNN, whereas the original WIND Toolkit uses the YSU scheme.
- **Time period**: The time period of simulation is another major difference; the new CA20 data set models a full 20 years (2000–2019), whereas the WTK modeled only the years 2007–2013.
- **Sea-surface temperature product**: The two data sets use different SST products. CA20 leverages the OSTIA 0.25-degree data set for model years 2007 and higher and the HadISST2 data set for the 2000–2006 model years; WTK uses the NCEP RTG 1/12-degree SST data set, which was discontinued in 2019.
- **WRF version**: Finally, the data sets use different versions of the WRF NWP model. The CA20 data set leverages a recent release of the WRF model, Version 4.1.2, whereas the WTK used Version 3.4, which was the state of the art in 2013.

Table 13. Comparison of Key Attributes Between WTK and CA20

Feature	WIND Toolkit	CA20
Reanalysis product	ERA-interim	ERA5
Planetary boundary layer scheme	YSU	MYNN
Time period	7 years (2007–2013)	20 years (2000–2019)
Sea-surface temperature product	NCEP RTG 1/12 degree	HadISST2 0.25 degree (pre-2007) OSTIA 0.25 degree (post-2007)
WRF version	3.4	4.1.2

4.2.1 Reanalysis Data

The ERA5 reanalysis data set is the latest state-of-the-art product released by ECMWF and now replaces ERA-interim. The code was released in 2016 and over the last 4 years, reanalysis data back to 1979 have been produced and disseminated. Table 14 summarizes the main differences between ERA5 and its predecessor ERA-interim. Most notable is the increased horizontal resolution from 79 km in ERA-interim to 31 km in ERA5—increasing by nearly a factor of 3. The number of vertical levels more than doubled from 60 to 137. Finally, the time frequency of the publicly released data increased from every 6 hours to hourly, allowing much better resolution of the large-scale flow.

Beyond the improvements highlighted in Table 14, an extensive range of physics, dynamics, and parameterization improvements went into ERA5. Discussion of these improvements is beyond the scope of this report, but can be found in Hersbach et al. 2020.

Table 14. Comparison of Key Attributes Between ERA-Interim and ERA5

Feature	ERA-Interim	ERA5
Model release	2006	2016
Horizontal resolution	79 km	31 km
Vertical resolution	60 levels	137 levels
Output frequency	6 hours	Hourly

In Figure 22, we compare the mean annual wind resource in 2017 when ERA5 and ERA-interim are used as boundary forcings to the WRF model. The figure shows that despite extensive improvements from ERA-interim to ERA5, there are only modest differences in the 100-m WRF-modeled wind speeds in the OCS.

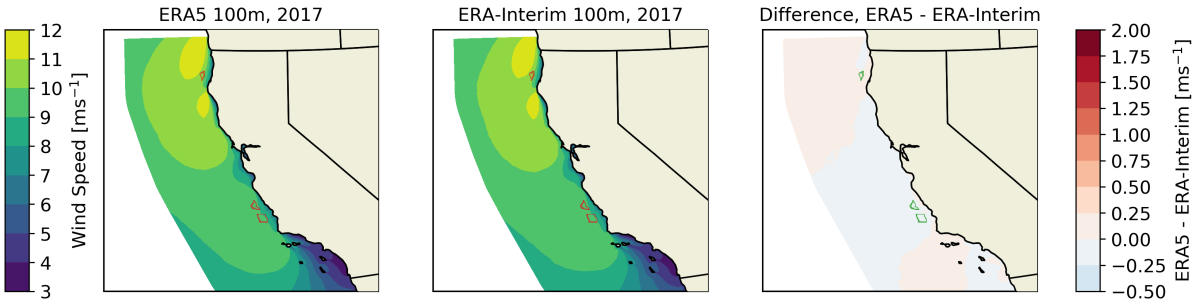

Figure 22. Mean 100-m wind speeds for the OCS modeled using WRF when forced by the ERA5 reanalysis product (left) and the ERA-interim reanalysis product (middle). The difference between the two modeled data sets is shown on the right. Call areas are shown in red (left and center) and green (right).

4.2.2 PBL Scheme

As detailed in Section 3, the use of MYNN and YSU schemes in WRF can have a substantial influence on the mean wind profile, especially in stable conditions. Figure 21 shows the difference in mean annual wind speeds for 2017 in the OCS when using MYNN compared to YSU. As shown in the figure, the use of MYNN results in higher wind speeds, particularly closer to the coastline, with increases of 1.02, 0.70, and 0.64 m·s^{-1} at the Humboldt, Morro Bay, and Diablo Canyon call areas, respectively.

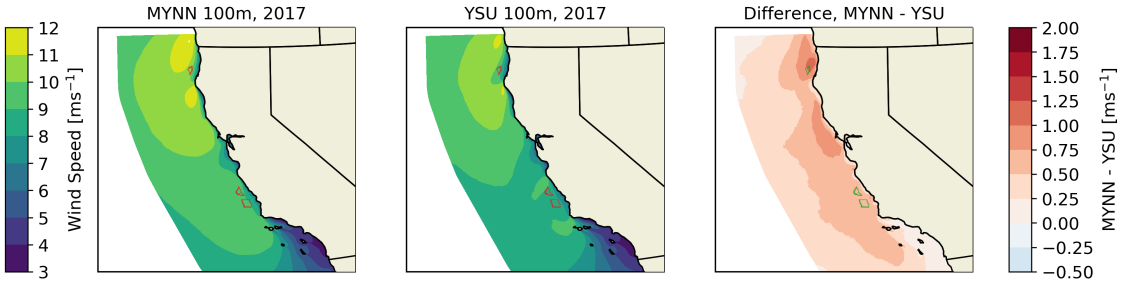

Figure 23. Comparison of mean 100-m wind speeds in 2017 when using MYNN (left) and YSU (middle) PBL schemes. The difference between the two is shown on the right. Call areas are shown in red (left and center) and green (right).

4.2.3 Time Period

The impact of modeling time period (i.e., use of 20 years in CA20 versus 7 years in WTK) is shown in Figure 24. Here, we plot the mean annual 100-m wind speeds from the CA20 data set over the full 2000–2019 data period and over the 2007–2013 period. As shown in the figure, there is an overall slight decrease in the mean resource when modeled over the full 20 years compared to the 7-year period, indicating that the 2007–2013 period had a slightly above-average wind resource. Overall, we find decreases of -0.08, -0.37, and -0.32 m·s^{-1} at the Humboldt, Morro Bay, and Diablo Canyon call areas, respectively.

We further investigate estimates of interannual variability (IAV) between the 20-year and 7-year periods. The IAV metric is defined as the expected variation of the wind resource from year to year, and is calculated as the standard deviation of annual wind speeds divided by the long-term mean. This IAV metric is a critical component of preconstruction energy estimates and a key source of risk for investing in new wind farm construction.

A comparison of IAV over the 20-year and 7-year time periods is shown in Figure 25. As shown in the figure, the two time periods model substantial differences in IAV, particularly in the middle of the domain, where we see differ-

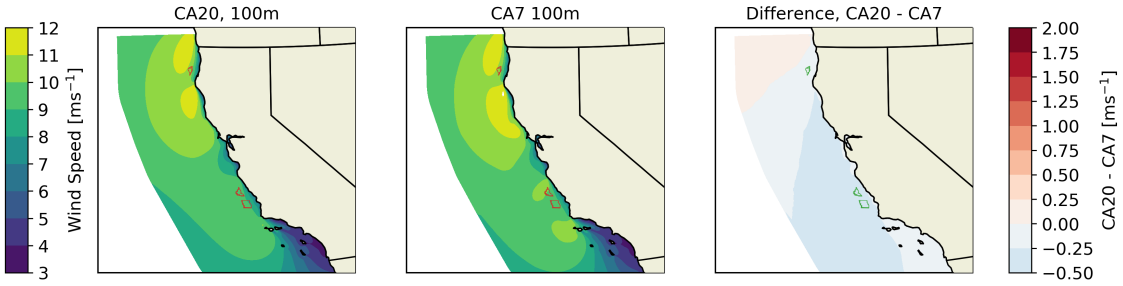

Figure 24. Comparison of mean long-term 100-m wind speeds in the CA20 wind resource data set when considering the full 20-year period (2000–2019; left) and only a 7-year period (2007–2013; center). The difference between the two is shown on the right. Call areas are shown in red (left and center) and green (right).

ences of 5% or greater. The impact is less at the wind energy call areas, where we find increases of around 1.0% to 1.5%.

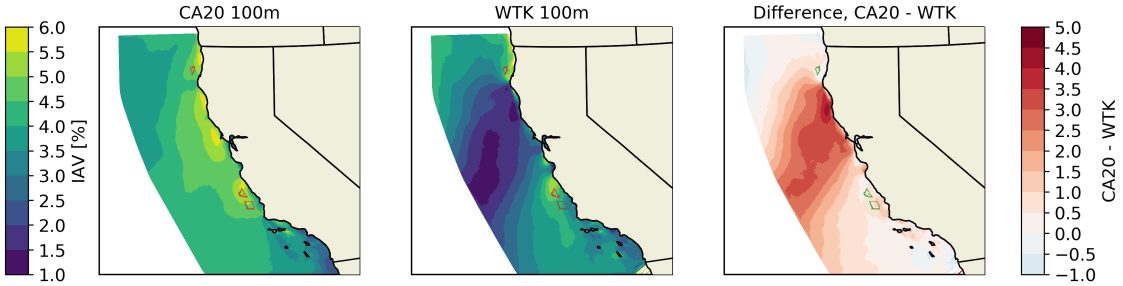

Figure 25. Comparison of interannual variability estimated from the CA20 data set (left) and the WTK (middle). The difference between the two is shown on the right. Call areas are shown in red (left and center) and green (right).

We explore the reason for the large increase in the central domain in Figure 26. Here, we plot the time series of annual wind speeds at Buoy 46014, where an increase of more than 5% IAV is observed using the full 20-year time period. The figure shows that the annual wind speeds during the WTK modeling period (2007–2013) were consistent with very low variability. Indeed, this period represents the most consistent wind speeds in the entire 20-year record. Outside this WTK modeling period, we observe much more variability in the wind resource.

This discrepancy in IAV highlights a key limitation of the 7-year WTK data set and the importance of a longer time period to more accurately capture the annual variability of the wind resource.

4.2.4 Sea-Surface Temperature Product

The impact of SST product (i.e., OSTIA in ERA5 and NCEP Real-Time Global in WTK) is shown in Figure 27. In general, the modeled resource is similar when different SST forcings are used, with differences across the OCS from -0.25 to 0.25 m·s^{-1}. For annual timescales, at least, the impact of SST product is relatively low.

4.2.5 WRF Version

The impact of WRF version (i.e., 4.1.2 for CA20 and 3.4.1 in WTK) is shown in Figure 28. There are some modest differences in the modeled resource between the two WRF versions, mostly ranging from -0.25 to 0.25 m·s^{-1}. For annual timescales, at least, the impact of WRF version is relatively low.

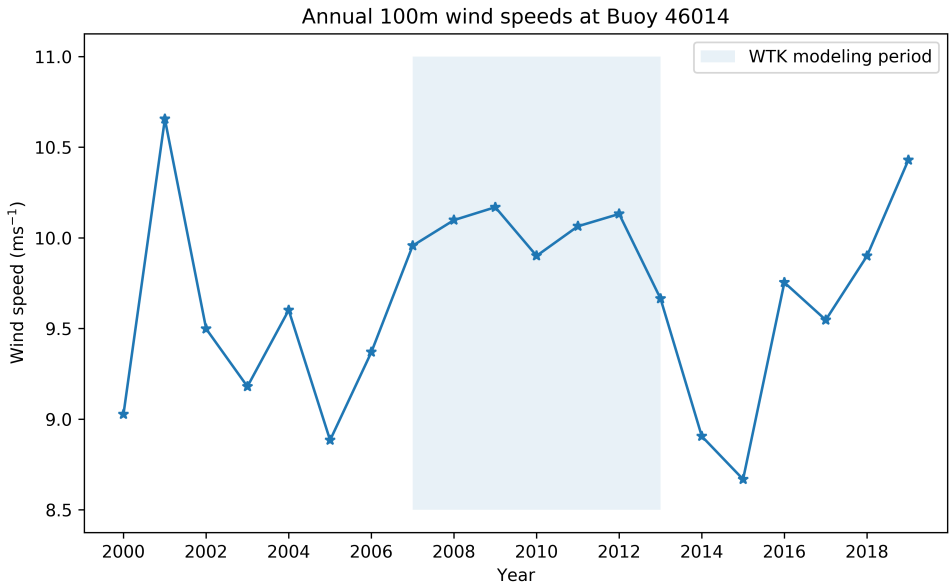

Figure 26. Mean annual wind speeds modeled from CA20 at Buoy 46014. The WTK period of record is shaded in blue.

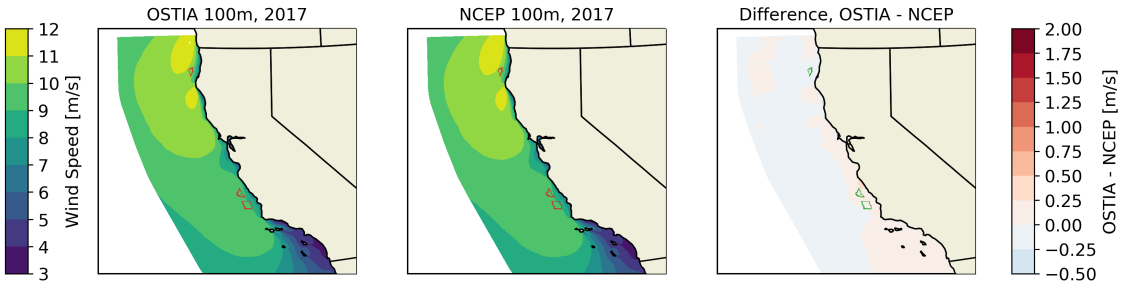

Figure 27. Comparison of mean long-term 100-m wind speeds in the new wind resource data set when using the OSTIA sea-surface temperature data set (left) and the NCEP RTG sea-surface tempterature data set (middle). The difference between the two is shown on the right. Call areas are shown in red (left and center) and green (right).

4.2.6 Combined Impact

In Figure 29, we combine the previous subsections to explore the combined impact of reanalysis product, PBL scheme, modeling time period, and SST product on explaining the increase in wind resource between CA20 and WTK. The figure shows that although most of the difference in the Northern California OCS is accounted for, there remains significant increases in the mid- and Southern California OCS not. Specifically, there remains an unexplained 0.98 and 1.11 m·s^{-1} increase at the Morro Bay and Diablo Canyon Call Areas; by contrast, only 0.17 m·s^{-1} is left unexplained at Humboldt.

There are several potential explanations for the unaccounted increase in the wind resource between CA20 and WTK:

- **WRF version**: The WTK used WRF Version 3.4, whereas CA20 used WRF Version 4.1.2. Given the extensive improvements across all aspects of the WRF model over the last 7 years, there are likely other model improvements not considered here that influence the wind resource (e.g., change to hybrid vertical coordinate

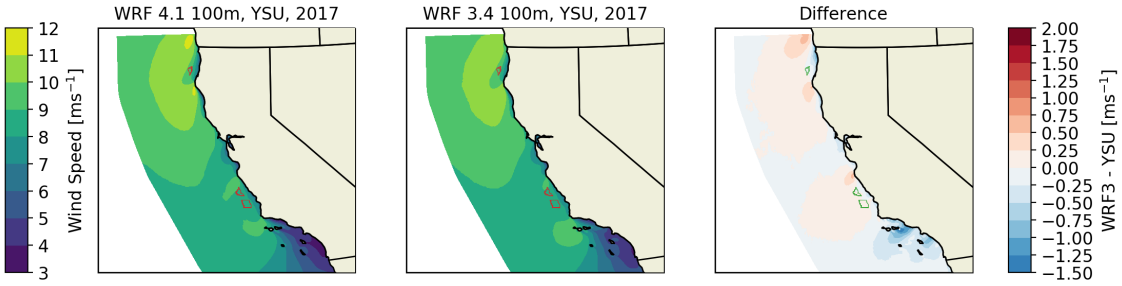

Figure 28. Comparison of mean long-term 100-m wind speeds in the new wind resource data set when using WRF version 4.1.2 (left) and WRF version 3.4.1 (middle). The difference between the two is shown on the right. Call areas are shown in red (left and center) and green (right).

system in WRF version 4.0).

- **Topographic data**: The WTK and CA20 model simulations used different topographic data sources: the WTK used the GTOPO30 data set from the U.S. Geological Survey (USGS) at a 30-second spatial resolution, whereas the CA20 data set used the next-generation GMTED2010 data set—a collaboration between USGS and the National Geospatial-Intelligence Agency—also at a 30-second spatial resolution.
- **Land-use data**: The WTK and CA20 model simulations used different land-use category data sets: the WTK used the National Land Cover Database (NLCD) at a 3-second spatial resolution, whereas CA20 used the MODIS 30-second resolution data.
- **Vertical resolution**: The WTK was run with 5 vertical levels below 200 m, whereas CA20 was run with 10 vertical levels. Higher vertical resolution near the surface can have a large impact on modeled wind speeds at hub height.

It is likely that these additional differences in model setup are driving some changes in the annual offshore wind resource. Further sensitivity analyses on these differences would be a good area for future study.

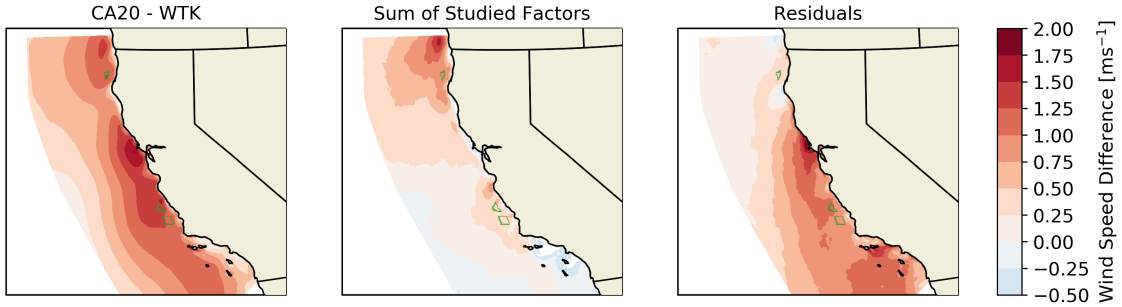

Figure 29. A summary of mean 100-m wind speed differences modeled between CA20 and WTK. The total difference is shown on the left. The explained difference in terms of reanalysis product, PBL scheme, time period, and SST product is shown in the middle. The remaining unexplained difference is shown on the right.

5 Quantifying Sensitivity in the Modeled Wind Resource

This section summarizes the approaches to quantifying sensitivity (i.e., the spread in the distribution of WRF model setups) in the new wind resource data set. Sensitivity is quantified in terms of the standard deviation of 100-m wind speed normalized by wind speed itself, and it calculated on annual and hourly scales.

5.1 WRF Ensemble Sensitivity in Wind Resource for 2017

The use of multiple WRF setups (i.e., ensemble members) for numerical modeling allows for a direct assessment of the sensitivity or variability in the modeled wind resource. The use of this metric is limited to 2017, the year during which WRF ensemble runs were performed.

This sensitivity metric is calculated using annual wind speed data (i.e., one value for each ensemble member at each location) and hourly average data (i.e., 8,760 values for each ensemble member at each location). At each time stamp at each grid point, the across-member standard deviation is calculated and normalized by the corresponding average wind speed. Then, the mean value at each location is taken.

Figure 30 shows maps of the obtained average values of sensitivity in 100-m wind speed, computed using annual and hourly average wind speed data. Sensitivity varies between 1% and 7% and is largest closest to the coast and within the wind energy call areas. Most of this sensitivity can be attributed to the choice of PBL scheme (MYNN or YSU) and the diverging wind profiles associated with each under strong stable atmospheric conditions near the coastline.

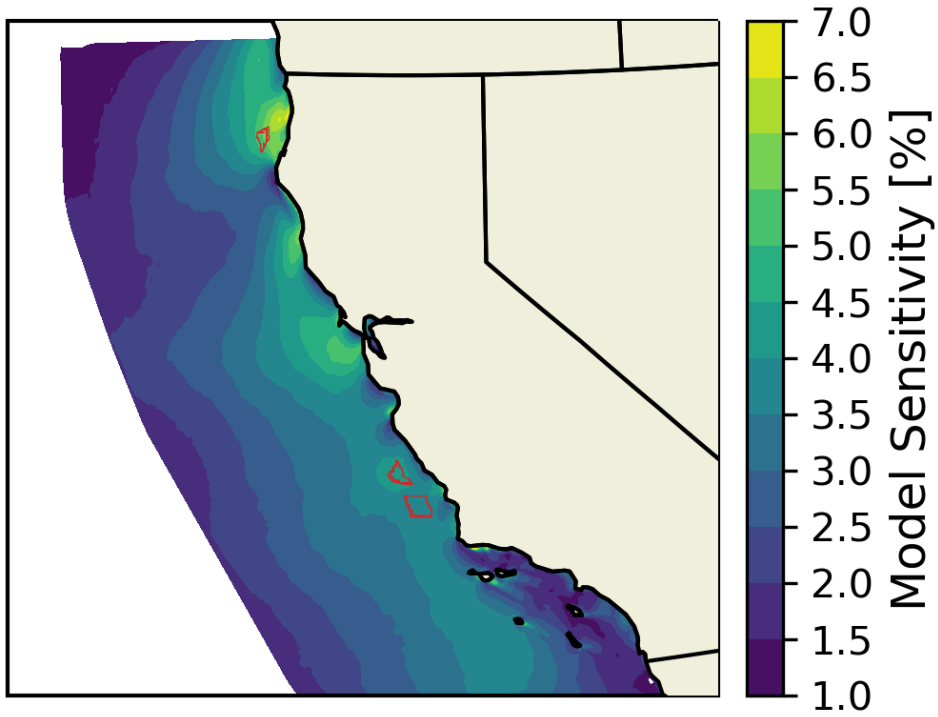

Figure 30. Mean annual sensitivity in 100-m wind speed quantified as an across-member normalized standard deviation from the 2017 ensemble runs

5.2 Extrapolation of Sensitivity in Wind Resource to 20-Year Period

Because of computational limitations, the ensemble runs produced in 2017 could not be run for the whole 20-year period. However, it is still valuable to provide high-resolution sensitivity metrics for the full long-term period. To address this problem, state-of-the-art techniques can be leveraged to extrapolate the hourly sensitivity in 100-m wind resource to the full 20-year period. Two different approaches are followed so that a confidence interval can be added to the proposed uncertainty extrapolation:

1. A machine-learning algorithm to extrapolate the WRF-based ensemble uncertainty from 2017 to the full 20-year period
2. An analog ensemble technique (e.g., Alessandrini et al. 2015) to quantify local sensitivity in wind resource from the spread in modeled cases with similar atmospheric conditions.

5.2.1 20-Year Wind Speed Uncertainty from Machine-Learning Approach

A machine-learning gradient-boosting algorithm is used to extrapolate the WRF ensemble spread calculated for the 2017 100-m wind speed to the full 20-year record of 100-m wind speeds. To do so, the machine-learning algorithm is trained to predict the hourly average ensemble standard deviation of 100-m wind speed, normalized by the 100-m wind speed itself. The following set of variables from the WRF runs are used as inputs to the learning model:

- Wind speed at 100 m above ground level (AGL)
- Wind direction at 100 m AGL
- Temperature at 40 m AGL
- Inverse of Obukhov length at 2 m AGL
- Standard deviation of 100-m wind speed calculated over the preceding 6 hours
- Standard deviation of 100-m wind speed calculated over the preceding 2 hours
- Shear exponent calculated between 200 m and 10 m AGL
- Time of day
- Month.

The gradient-boosting model is trained at each grid location using the 2017 data and then applied to predict the 100-m wind speed normalized standard deviation for the full 20-year period. The algorithm is trained using the coefficient of determination, R^2, as the performance metric to tune the model weights. Randomized cross validation is used to adapt the hyperparameters[1] to optimize the model performance while avoiding overfitting. The considered hyperparameters and the ranges of values sampled in the cross validation are reported in Table 15.

Table 15. Hyperparameters Considered in the Gradient-Boosting Model and Range of Values Sampled for Each in the Cross Validation

Hyperparameter	Values Sampled
Learning rate	From 0.05 to 1
Maximum tree depth	From 4 to 10
Maximum number of features	From 1 to 7
Minimum number of samples to split	From 2 to 20
Minimum number of samples for a leaf	From 1 to 20
Number of estimators	From 100 to 300

[1]Hyperparameters are algorithm parameters that are set before the learning process begins

Figure 31 shows the 100-m wind speed uncertainty for the region surrounding the Humboldt lease area, calculated as the median value of the hourly prediction for the full 20-year period. Sensitivity in wind speed increases closer to land, with values greater than 20% at the hourly scale. In the region of interest for the Humboldt lease, median uncertainty in hourly wind speed ranges between 11% and 12%.

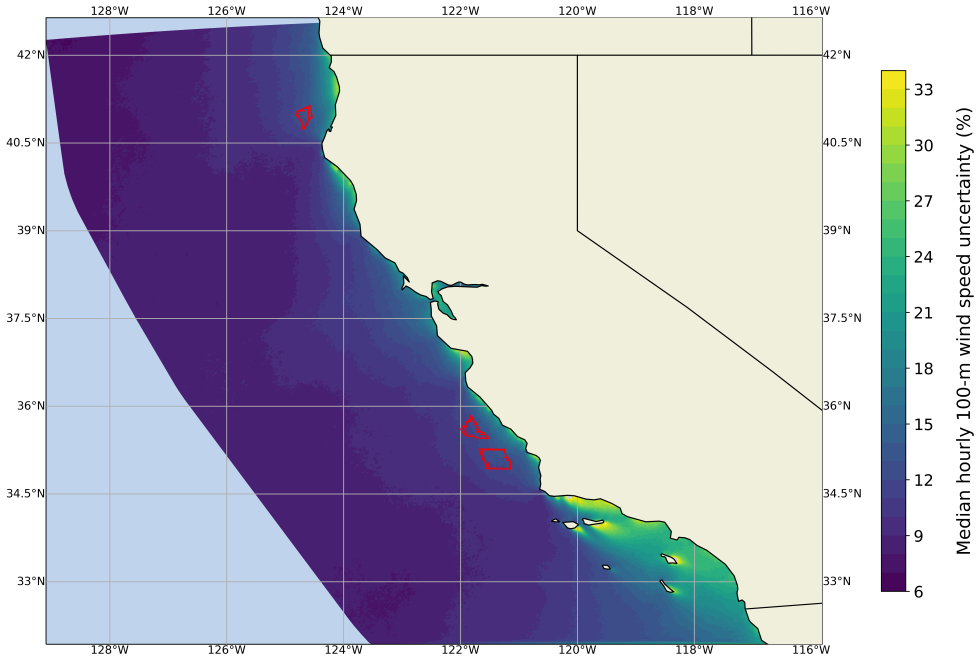

Figure 31. Median hourly uncertainty in 100-m wind speed as derived from the machine-learning approach applied to the full 20-year period.

5.2.2 20-Year Wind Speed Uncertainty from Analog Ensemble Approach

The second approach applied to quantify long-term hourly wind speed uncertainty uses an analog ensemble (AnEn) technique (Alessandrini et al. 2015). With this approach, at each site, the value of multiple physical variables (the same inputs used in the machine-learning model, except for time of day and month) is retrieved for a time window centered around each hourly time stamp. Then, analog windows are identified as other historical cases with conditions similar to those in the target window and occurring around the same hour of the day. The analogs are ranked by closeness of match. The 20 best analogs are chosen, and the corresponding modeled values of 100-m wind speed saved. The choice of using 20 analogs is justified to resemble the number of WRF ensemble members used in the numerical modeling. In computing the closeness of match metric to identify the analogs, relative weights are assigned to the various physical variables considered, as shown in Table 16.

The final result of this approach is the analog ensemble, which is a set of 20 hourly average wind speed values for each time stamp at each location. It is assumed that the spread of the 20 analogs can be considered as a proxy of the uncertainty in wind resource. The standard deviation of the 20 analog values, normalized by their average, is then calculated and used as metric to quantify this uncertainty. Research into the analog ensemble method is still ongoing; therefore, we present preliminary results for the area around the Humboldt Call Area.

Figures 32 and 33 contrast the machine-learning and analog ensemble-based approaches around the Humboldt Call Area. As found with the machine-learning approach, sensitivity in wind speed increases closer to land. Overall, the values found with the analog ensemble (ranging from about 4% to 11%) are substantially smaller than what was estimated with the machine-learning approach (ranging from about 9% to 25%). Reasons for these differences will be the focus of future analysis.

Table 16. Weights Given to Each Physical Variable in Computing the Closeness of Match Metric to Identify the Analogs

Physical Variable	AnEn Weight
Wind speed at 100 m AGL	0.5
Wind direction at 100 m AGL	0.2
Temperature at 40 m AGL	0.05
Inverse of Obukhov length at 2 m AGL	0.05
Standard deviation of 100-m wind speed over preceding 6 hours	0.05
Standard deviation of 100-m wind speed over preceding 2 hours	0.1
Shear exponent calculated between 200 m and 10 m AGL	0.05

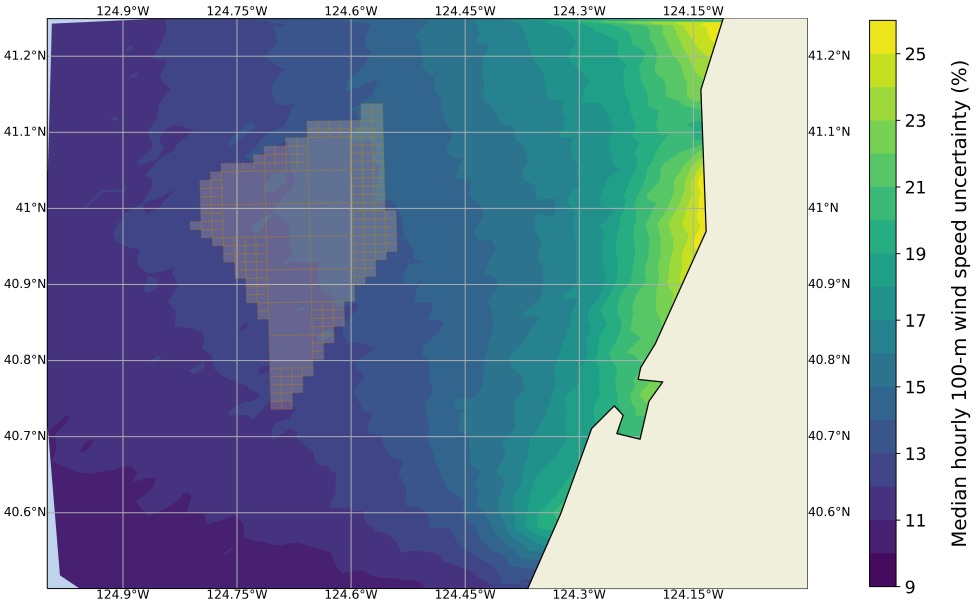

Figure 32. Median hourly uncertainty in 100-m wind speed around the Humboldt Call Area (grey) as derived from the machine-learning approach applied to the full 20-year period.

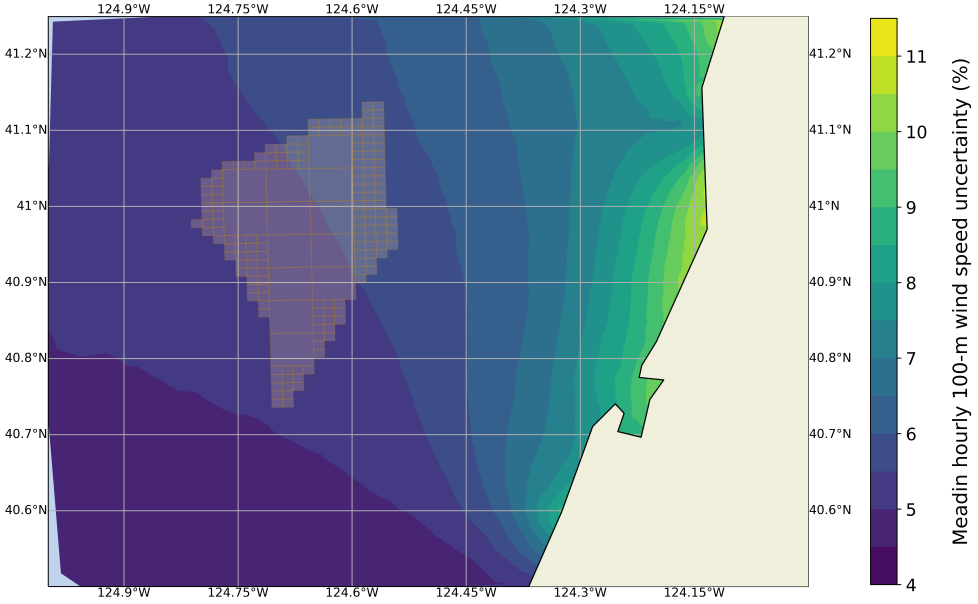

Figure 33. Median hourly uncertainty in 100-m wind speed around the Humboldt Call Area (grey) as derived from the Analog Ensemble (AnEn) approach applied to the full 20-year period

6 Summary and Key Findings

This report presents a state-of-the-art wind resource data set by NREL for the OCS. This CA20 data set is intended to be used in place of NREL's WIND Toolkit, which was produced and released publicly in 2013 and is currently the principal data set used by stakeholders for wind resource assessment in the OCS. This update to the OCS wind resource data set is part of a larger study funded by BOEM that will provide an updated cost model for floating offshore wind in the OCS. This work is also part of a broader effort to replace NREL's WIND Toolkit using the 20-year, ensemble-based modeling approach employed here.

The CA20 data set improves upon the WIND Toolkit through:

1. A 20-year modeling period from 2000 through 2019 (compared to the 7-year 2007–2013 modeling period in the WIND Toolkit)
2. A sensitivity analysis of the hub-height wind resource, driven by an ensemble of 16 different WRF simulations run in the 2017 calendar year
3. An updated WRF version, from Version 3.4 used in the WIND Toolkit to Version 4.1.2 used here, which incorporates significant R&D advancements
4. The use of the state-of-the-art reanalysis product ERA5 to provide atmospheric forcing at the WRF domain boundaries. The ERA5 product is produced by the ECMWF and replaces its older ERA-interim product, which was used in the WIND Toolkit.

This report found significantly higher mean wind speeds modeled in the new data set compared to the WIND Toolkit. In some areas, the increase approaches and even exceeds 2 $m \cdot s^{-1}$, or an increase of about 20%. Increases in the estimated mean 100-m wind speed at the centroids of current wind energy call areas are 9.7%, 17.4%, and 19.7% at Humboldt, Morro Bay, and Diablo Canyon, respectively.

This increase in the modeled wind resource is significant and will impact economic and energy modeling and planning for offshore wind in the OCS. Therefore, this report largely focuses on explaining and justifying this increase in the modeled resource, primarily through validation against observation and examining the underlying differences between the new CA20 data set and the WIND Toolkit model setups.

Based on this detailed analysis, much of the increase in the modeled wind resource can be attributed to an updated PBL scheme. The WIND Toolkit used the YSU scheme, whereas the new data set uses the MYNN scheme. The MYNN scheme has become the global standard and has been the subject of significant research and development over the past decade. The use of the MYNN scheme produces significantly higher hub-height wind speeds than YSU, which can be attributed to the high frequency of stable atmospheric conditions in the OCS and the divergence of these PBL schemes under such conditions.

This increase in the modeled wind resource leads to an increase in estimated technical potential for the OCS. The new technical potential is compared against the values quantified in NREL's 2016 report on the U.S. offshore wind resource (Musial et al. 2016). The increased wind resource in the new data set leads to a 4.7% increase in area-based and capacity-based technical potential, which can be attributed to a slightly larger OCS area that exceeds 7 $m \cdot s^{-1}$.

Finally, the significant increase in the modeled wind resource compared to the WIND Toolkit highlights the spread of NWP-modeled wind speeds to model inputs and setup. To quantify the sensitivity of this modeled OCS wind resource data set, NREL considered an ensemble of 16 WRF setups ran in the 2017 calendar year that vary in the inputs and model parameterizations within WRF. These setups account for different reanalysis products as boundary forcing, different PBL schemes, different SST forcing products, and different land surface schemes. Sensitivity in the annual 100-m wind resource was found to be 5% to 7% across the OCS wind energy Call Areas. These values can be interpreted as confidence in the modeled wind resource at each grid point. Sensitivity calculated for the 2017 calendar year was then extended to the 20-year data set by training a machine-learning model to predict this sensitivity based on key modeled atmospheric variables. This novel approach developed by NREL is then contrasted

against a more typical analog ensemble approach in which wind speed spread or sensitivity is deduced from a single model run without the use of actual ensembles.

7 Recommendations for Future Analysis

7.1 The OCS Wind Resource

This analysis reveals that the OCS is characterized by high frequencies of stable atmospheric conditions, which have a significant impact on the wind profile. A detailed analysis of OCS wind conditions under such stability was beyond the scope of this analysis; however, it is likely that strong low-level jets and high-shear events are common in the OCS. This high frequency of stable conditions, which is most common near the coastline, is likely caused by upwelling of cold water to the surface along the coast, which cools the air near the ocean surface and induces a stable stratification.

NREL recommends future work to fully characterize the wind resource under such unique meteorological conditions. An analysis of floating lidar data (to be deployed in the near future by DOE) and comparison against the WRF model would highlight how well these highly stable conditions can be modeled and how accurately WRF can predict low-level jets and other events associated with this phenomenon. Such lidar data would also be extremely valuable in validating the CA20 data set.

In addition, now that a 20-year wind resource data set has been produced, a detailed analysis of wind and solar resources can be performed for the OCS. NREL's National Solar Radiation Database contains more than 20 years of estimated solar irradiance from satellite measurements. These data, combined with the new 20-year wind resource data set, can be used to explore how the wind resource in different parts of the OCS can complement the solar resource and mediate the well-known "duck curve" in California, where the solar resource decreases in the late afternoon and evenings just as demand is increasing.

7.2 Extending New Data Set to More Offshore Domains

This new wind resource data set for the OCS highlights the advancement of NWP modeling capabilities at NREL. The creation of a 20-year data set, as well as 16 ensemble setups run over a year, are made possible by investment in both computational resources and atmospheric science expertise at the lab. The methods and framework developed to produce this new data set are currently being leveraged to begin the full replacement of the national-scale WIND Toolkit, which is expected to be complete by 2022. However, 20-year data sets for key U.S. offshore areas (e.g., Atlantic, Hawaii, Oregon) will be completed in late 2020 to early 2021 to further support the U.S. offshore wind industry.

Given the rapid pace of R&D in NWP science, with an emphasis on improving offshore wind resource modeling, NREL anticipates the need to continually update its wind resource modeling capabilities and products, likely through 5- to 7-year update periods. These frequent updates will ensure that NREL is producing the most accurate and comprehensive wind resource data sets for both its U.S. and global wind energy stakeholders.

References

Alessandrini, S., et al. 2015. "A novel application of an analog ensemble for short-term wind power forecasting". *Renewable Energy* 76:768 –781. ISSN: 0960-1481. doi:https://doi.org/10.1016/j.renene.2014.11.061. http://www.sciencedirect.com/science/article/pii/S0960148114007915.

Benjamin, Stanley G., et al. 2016. "A North American Hourly Assimilation and Model Forecast Cycle: The Rapid Refresh". _eprint: https://journals.ametsoc.org/mwr/article-pdf/144/4/1669/4334616/mwr-d-15-0242_1.pdf, *Monthly Weather Review* 144 (4): 1669–1694. ISSN: 0027-0644. doi:10.1175/MWR-D-15-0242.1. https://doi.org/10.1175/MWR-D-15-0242.1.

Bosilovich, Michael. 2015. "MERRA-2: Initial Evaluation of the Climate". 43:145.

Carvalho, D., et al. 2014a. "Offshore wind energy resource simulation forced by different reanalyses: Comparison with observed data in the Iberian Peninsula". *Applied Energy* 134:57 –64. ISSN: 0306-2619. doi:https://doi.org/10.1016/j.apenergy.2014.08.018. http://www.sciencedirect.com/science/article/pii/S0306261914008216.

– . 2014b. "Sensitivity of the WRF model wind simulation and wind energy production estimates to planetary boundary layer parameterizations for onshore and offshore areas in the Iberian Peninsula". *Applied Energy* 135:234 –246. ISSN: 0306-2619. doi:https://doi.org/10.1016/j.apenergy.2014.08.082. http://www.sciencedirect.com/science/article/pii/S0306261914008939.

Donlon, Craig J., et al. 2012. "The Operational Sea Surface Temperature and Sea Ice Analysis (OSTIA) system". *Remote Sensing of Environment*, Advanced Along Track Scanning Radiometer(AATSR) Special Issue, 116 (): 140–158. ISSN: 0034-4257, visited on 06/21/2020. doi:10.1016/j.rse.2010.10.017. http://www.sciencedirect.com/science/article/pii/S0034425711002197.

Draxl, Caroline, and Bri-Mathias Hodge. 2015. "Wind Integration National Dataset (WIND) Toolkit; NREL (National Renewable Energy Laboratory)" ().

Draxl, Caroline, et al. 2015. "The Wind Integration National Dataset (WIND) Toolkit". *Applied Energy* 151:355 –366. ISSN: 0306-2619. doi:https://doi.org/10.1016/j.apenergy.2015.03.121. http://www.sciencedirect.com/science/article/pii/S0306261915004237.

Gelaro, Ronald, et al. 2017. "The Modern-Era Retrospective Analysis for Research and Applications, Version 2 (MERRA-2)". _eprint: https://journals.ametsoc.org/jcli/article-pdf/30/14/5419/4676847/jcli-d-16-0758_1.pdf, *Journal of Climate* 30 (14): 5419–5454. ISSN: 0894-8755. doi:10.1175/JCLI-D-16-0758.1. https://doi.org/10.1175/JCLI-D-16-0758.1.

Gómez-Navarro, J. J., C. C. Raible, and S. Dierer. 2015. "Sensitivity of the WRF model to PBL parametrisations and nesting techniques: evaluation of wind storms over complex terrain". *Geoscientific Model Development* 8 (10): 3349–3363. doi:10.5194/gmd-8-3349-2015. https://www.geosci-model-dev.net/8/3349/2015/.

Grumbine, Robert. 2020. *Description of NCEP High Res. SST Analysis*. Library Catalog: polar.ncep.noaa.gov. Visited on 06/21/2020. https://polar.ncep.noaa.gov/sst/rtg_high_res/description.shtml.

Hahmann, A. N., et al. 2020. "The Making of the New European Wind Atlas, Part 1: Model Sensitivity". *Geoscientific Model Development Discussions* 2020:1–33. doi:10.5194/gmd-2019-349. https://www.geosci-model-dev-discuss.net/gmd-2019-349/.

Hahmann, Andrea N., et al. 2015. "Wind climate estimation using WRF model output: method and model sensitivities over the sea". *International Journal of Climatology* 35 (12): 3422–3439. doi:10.1002/joc.4217. eprint: https://rmets.onlinelibrary.wiley.com/doi/pdf/10.1002/joc.4217. https://rmets.onlinelibrary.wiley.com/doi/abs/10.1002/joc.4217.

Hersbach, Hans, et al. 2020. "The ERA5 global reanalysis". *Quarterly Journal of the Royal Meteorological Society* (): qj.3803. ISSN: 0035-9009, 1477-870X, visited on 06/21/2020. doi:10.1002/qj.3803. https://onlinelibrary.wiley.com/doi/abs/10.1002/qj.3803.

Hirahara, S., et al. 2016. *Sea Surface Temperature and Sea Ice Concentration for ERA5*. Publisher: ECMWF Series: ERA Report.

Jiménez, Pedro A., et al. 2012. "A Revised Scheme for the WRF Surface Layer Formulation". _eprint: https://journals.ametsoc.org/mwr pdf/140/3/898/4271123/mwr-d-11-00056_1.pdf, *Monthly Weather Review* 140 (3): 898–918. ISSN: 0027-0644. doi:10.1175/MWR-D-11-00056.1. https://doi.org/10.1175/MWR-D-11-00056.1.

Kalverla, Peter C., et al. 2020. "Quality of wind characteristics in recent wind atlases over the North Sea". _eprint: https://rmets.onlinelibrary.wiley.com/doi/pdf/10.1002/qj.3748, *Quarterly Journal of the Royal Meteorological Society* 146 (728): 1498–1515. ISSN: 1477-870X, visited on 06/15/2020. doi:10.1002/qj.3748. https://rmets.onlinelibrary.wiley.com/doi/abs/10.1002/qj.3748.

León, José Andrés Pérez. 2019. *Global reanalysis: goodbye ERA-Interim, hello ERA5*. Text. Library Catalog: ecmwf.net. Visited on 06/21/2020. https://www.ecmwf.int/en/newsletter/159/meteorology/global-reanalysis-goodbye-era-interim-hello-era5.

Musial, Walt, et al. 2016. "2016 Offshore Wind Energy Resource Assessment for the United States" (). doi:10.2172/1324533.

Niu, Guo-Yue, et al. 2011. "The community Noah land surface model with multiparameterization options (Noah-MP): 1. Model description and evaluation with local-scale measurements". _eprint: https://agupubs.onlinelibrary.wiley.com/doi/pdf/1 *Journal of Geophysical Research: Atmospheres* 116 (D12). ISSN: 2156-2202, visited on 06/21/2020. doi:10.1029/2010JD015139. https://agupubs.onlinelibrary.wiley.com/doi/abs/10.1029/2010JD015139.

Olsen, B. T., et al. 2017. "An intercomparison of mesoscale models at simple sites for wind energy applications". *Wind Energy Science* 2 (1): 211–228. doi:10.5194/wes-2-211-2017. https://www.wind-energ-sci.net/2/211/2017/.

Optis, Michael, et al. 2020. "Validation of RU-WRF, the Custom Atmospheric Mesoscale Model of the Rutgers Center for Ocean Observing Leadership" (). doi:10.2172/1599576.

Ruiz, Juan J., Celeste Saulo, and Julia Nogués-Paegle. 2010. "WRF Model Sensitivity to Choice of Parameterization over South America: Validation against Surface Variables". *Monthly Weather Review* 138 (8): 3342–3355. doi:10.1175/2010MWR3358.1. https://doi.org/10.1175/2010MWR3358.1.

Shaw, William J., et al. 2019. "The Second Wind Forecast Improvement Project (WFIP2): General Overview". _eprint: https://journals.ametsoc.org/bams/article-pdf/100/9/1687/4871688/bams-d-18-0036_1.pdf, *Bulletin of the American Meteorological Society* 100 (9): 1687–1699. ISSN: 0003-0007. doi:10.1175/BAMS-D-18-0036.1. https://doi.org/10.1175/BAMS-D-18-0036.1.

Siuta, David, Gregory West, and Roland Stull. 2017. "WRF Hub-Height Wind Forecast Sensitivity to PBL Scheme, Grid Length, and Initial Condition Choice in Complex Terrain". *Weather and Forecasting* 32 (2): 493–509. doi:10.1175/WAF-D-16-0120.1.

Skamarock, C., et al. 2019. "A Description of the Advanced Research WRF Model Version 4". Visited on 06/21/2020. doi:10.5065/1dfh-6p97. https://opensky.ucar.edu/islandora/object/technotes%3A576/.

Ulazia, Alain, Jon Saenz, and Gabriel Ibarra-Berastegui. 2016. "Sensitivity to the use of 3DVAR data assimilation in a mesoscale model for estimating offshore wind energy potential. A case study of the Iberian northern coastline". *Applied Energy* 180:617 –627. ISSN: 0306-2619. doi:https://doi.org/10.1016/j.apenergy.2016.08.033. http://www.sciencedirect.com/science/article/pii/S0306261916311205.

Wilczak, James, et al. 2015. "The Wind Forecast Improvement Project (WFIP): A Public–Private Partnership Addressing Wind Energy Forecast Needs". _eprint: https://journals.ametsoc.org/bams/article-pdf/96/10/1699/3742802/bams-d-14-00107_1.pdf, *Bulletin of the American Meteorological Society* 96 (10): 1699–1718. ISSN: 0003-0007. doi:10.1175/BAMS-D-14-00107.1. https://doi.org/10.1175/BAMS-D-14-00107.1.

"WRF wind simulation and wind energy production estimates forced by different reanalyses: Comparison with observed data for Portugal". 2014. *Applied Energy* 117:116 –126. ISSN: 0306-2619. doi:https://doi.org/10.1016/j.apenergy.2013.12.001. http://www.sciencedirect.com/science/article/pii/S0306261913009847.

8 Appendix

8.1 Validating With Coastal Measurements

As discussed in Section 3, the use of coastal stations for offshore wind resource characterization and model validation is not ideal. Coastal stations are located far from current offshore wind energy lease areas and can have very different wind resource characteristics than those farther offshore. More importantly, large wind speed gradients at the coastline generally prohibit a meaningful validation of mesoscale-modeled wind speeds when these models are run at coarse resolution (e.g., 2-km resolution in the WIND Toolkit). Under these conditions, modeled wind speed from one model grid box to the next can change significantly, and the interpolation of modeled wind speeds to the observation station for purposes of validation is highly uncertain.

Figure 34 illustrates this coastal gradient problem at the McKinleyville radar station. The figure shows a 2-by-2-km grid of mean annual 200-m wind speeds from the WRF in 2017. The radar station is located in an area of high coastal gradients in which wind speeds in neighboring grid boxes can vary by over 1 $m \cdot s^{-1}$. Therefore, validating different model setups—where model differences in mean annual wind speeds can be on the order of 0.25 $m \cdot s^{-1}$ or less—can be difficult if not unreliable at coastal stations.

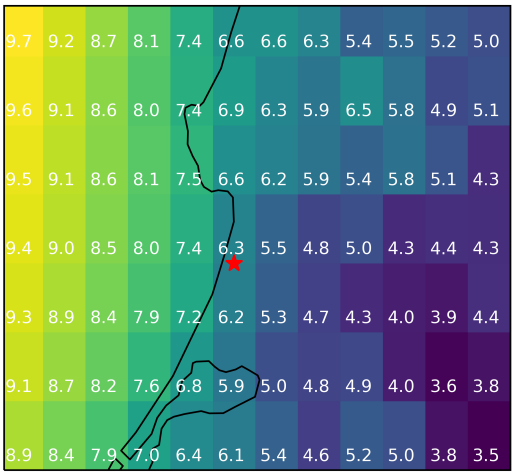

Figure 34. Mean annual wind speeds in 2017 at the McKinleyville radar site (red star), modeled in 2-km grid boxes by WRF

8.2 Ensemble Validation

Heat maps of unbiased RMSE, bias, and EMD for each WRF model setup at each of the OCS observation stations are shown in Figures 35–37.

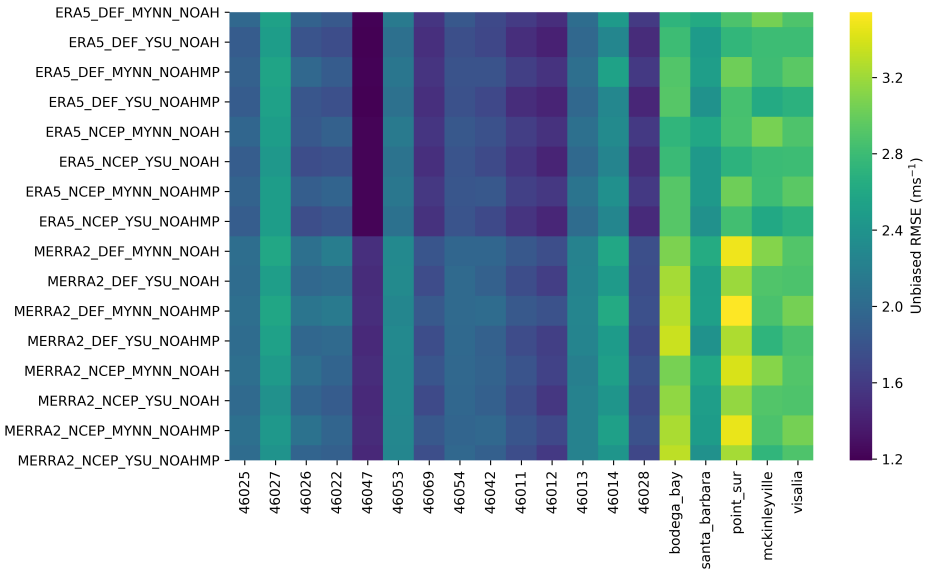

Figure 35. Unbiased RMSE for each WRF model setup at each of the observation stations

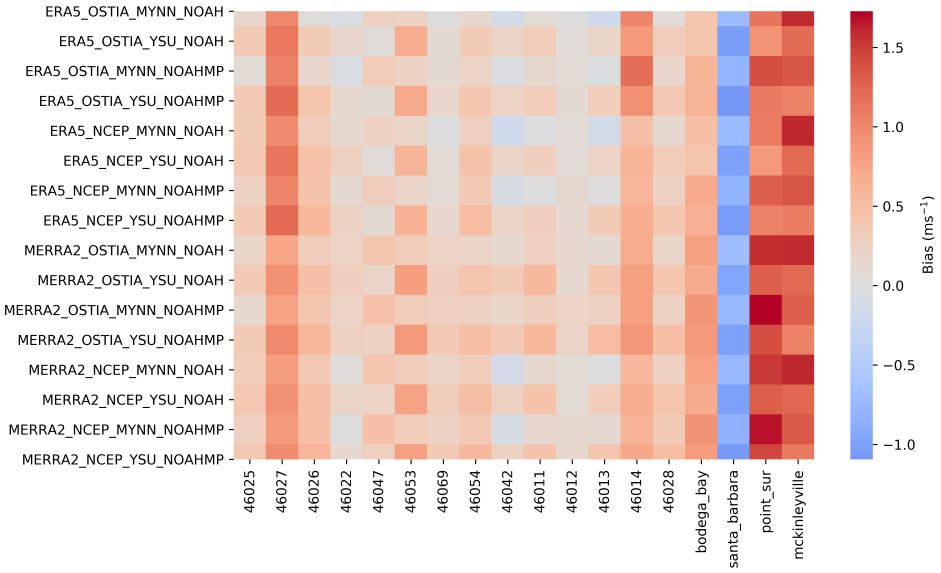

Figure 36. Bias for each WRF model setup at each of the observation stations

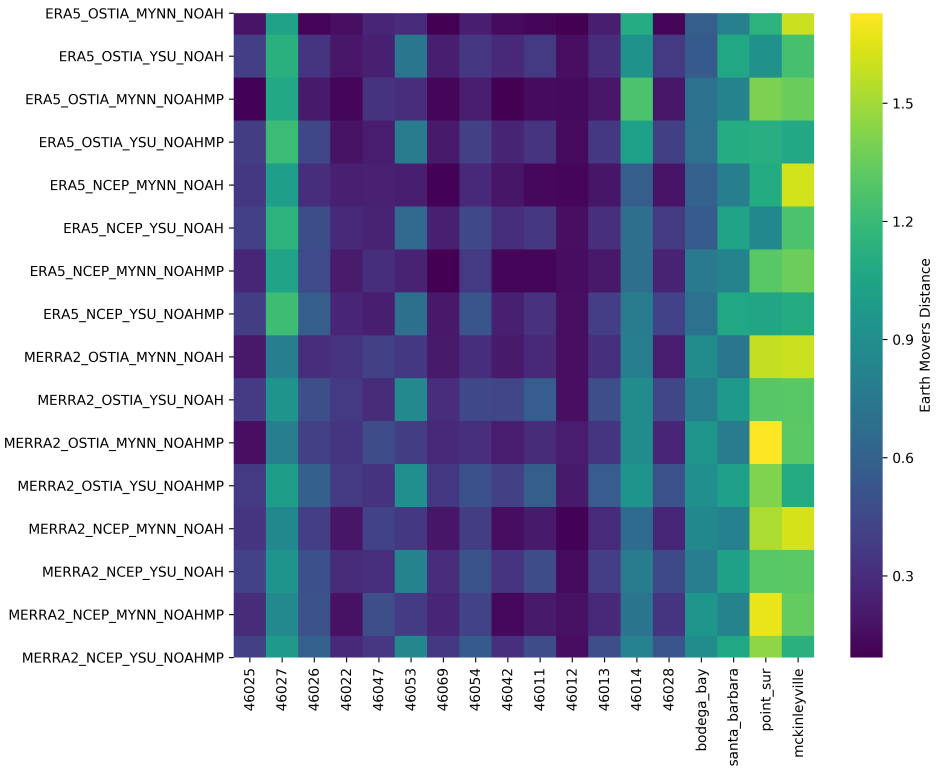

Figure 37. EMD for each WRF model setup at each of the observation stations